BONE SURFACE MIMICKED BIODEGRADABLE POLYMERIC SCAFFOLDS

by

ÖZNUR DEMİR

B.S., Biomedical Engineering, Yeditepe University, 2011

Submitted to the Institute of Biomedical Engineering
in partial fulfillment of the requirements
for the degree of
Master of Science
in
Biomedical Engineering

Boğaziçi University
2014

ACKNOWLEDGMENTS

I would like to express my appreciation and special thanks to my advisor Asist. Prof. Dr. Bora Garipcan. I would like to thank him for encouraging me in my research and for inspiring me to become a research scientist. I would also like to thank to my committee members, Assoc. Prof. Dr. Burak Güçlü and Assoc. Prof. Dr. Kadriye Tuzlakoğlu.

I would like to thank to PEDI-STEM Stem Cell Laboratory of Hacettepe University for helping cell studies of the thesis. Also, I would like to thank to Bogazici University R&D Center Electron Microscopy and Microanalysis Unit staff Dr. Bilge Gedik Uluocak.

In addition, I would like to give special thanks to my family. I always have felt their prayers on me during my thesis work. Morover, I would like to express appreciation to my beloved boyfriend Can Oğuz who always supported me and helped a lot to finish my thesis.

Furthermore, I would like to thank to Özgen Öztürk for sharing the same stress during her thesis. I would also like to thank my friends, Ayşegül Tümer, Bengü Aktaş, Selin Yalvarmış who supported me in every stage of this thesis. In the end, I would also give my thanks to my laboratory colleagues in developing the project.

ABSTRACT

BONE SURFACE MIMICKED BIODEGRADABLE POLYMERIC SCAFFOLDS

In this thesis, bone surface topography was mimicked by a using biodegradable polymer. In the first part, bone surface topography was mimicked and transferred to the polydimethylsiloxane (PDMS) surface using soft lithography technique. Bone surface mimicked Polylactic acid (BSM-PLA) prepared by solvent casting using the PDMS as a mold. The effect of PLA concentration (2.5-10% (w/v) in chloroform) and casting time (as evaporated-24 h) were investigated to obtain best mimicking conditions. After characterization of BSM-PLA scaffolds by scanning electron microscopy (SEM), the best mimicked scaffolds were obtained at 10% PLA concentration and 24 h casting time. The effectiveness of bone mimicking procedure was also investigated by SEM. As a result, same bone and PDMS surface could be used several times to fabricate BSM-PLA scaffolds. The fabricated BSM-PLA scaffolds' surface characterization results showed that the fabricated BSM-PLA surface hydrophobicity and roughness were improved to guide cells attachment. In second part, in-vitro degradation in terms of weight loss and morphology, and cumulative drug release tests were performed. Compared with the BSM-PLA, plain PLA scaffolds degraded more rapidly in phosphate buffer solution (PBS). The result was the same for the rate of drug release profile in PBS as well. For the last part of the thesis, the effect of surface topography on human bone marrow mesenchymal stem cells (hBM MSCs) viability and differentiation were investigated using BSM-PLA scaffolds. According to these results, stem cell incorporation onto BSM scaffolds as a future trend is addressed shortly highlighting the immense potential for osteogenic stem cell differentiation that features high adaptiveness to the biological environment. Consequently, the developed BSM-PLA scaffolds are predicted to have a great potential on the surface 3D scaffolds fabrication and guidance of stem cells that are provided for bone tissue engineering applications.

Keywords: Biomimetic, Bone tissue engineering, Stem cells.

ÖZET

KEMİK YÜZEYİ TAKLİT BİYOBOZUNUR POLİMERİK DOKU İSKELELERİ

Bu tez çalışmasında, kemik yüzey topoğrafyası biyobozunur bir polimer ile taklit edilmiştir. İlk bölümde, kemik yüzey topoğrafyasi taklit edilmiş ve yumuşak litografi tekniği kullanılarak polidimetilsiloksanın (PDMS) yüzeyine aktarılmıştır. Elde edilen PDMS kalıbı kullanılarak kemik yüzeyi taklit PLA (KYT-PLA) doku iskeleri hazırlanmıştır. En iyi taklit koşullarını belirlemek için, PLA doku iskelelerinin derişimi (%2.5-10.0 w/v) ve bekleme süresinin (buharlaşıncaya kadar-24 saat) etkisi taramalı elektron mikroskobu (SEM) kullanılarak incelenmiştir. SEM karakterizasyonu sonucunda %10 PLA derişimi ve 24 saat bekleme süresi en iyi taklit koşulları olarak belirlenmiştir. Kemik yüzeyi taklit prosedürünün etkinliği de SEM ile incelenmiştir. Sonuç olarak, KYT-PLA doku iskeleleri aynı kemik ve PDMS yüzeyi bir çok kez kullanılarak elde edilmiştir. Elde edilen KYT-PLA doku iskelelerinin yüzey karakterizasyon sonuçları, yüzey hidrofobikliği ve pürüzlülüğünün hücre tutunmasına olanak sağlayacak şekilde geliştirildiğini göstermiştir. İkinci bölümde, in-vitro bozunma çalışmaları kütle kaybı ve morfolojik olarak, ve kümülatif ilaç salınım testleri yapılmıştır. Düz PLA doku iskeleleri, KYT-PLA doku iskelelerine göre fosfat tompon çözeltisi (PBS) içerisinde daha hızlı bozunmuştur. İlaç salınım profil oranlarında da aynı sonuç görülmüştür. Tezin son bölümünde, yüzey topoğrafyasının insan kemik iliği mezenkimal kök hücrelerinin (hBM MSCs) canlılığı ve farklılaşmasına etkisi elde edilen KYT-PLA doku iskeleleri kullanılarak incelenmiştir. Bu sonuçlar, KYT doku iskeleleri üzerinde kök hücre etkileşiminin gelecek vaadeden bir çalışma olduğunu ve osteojenik kök hücre farklılaşma potansiyeli ile bunun biyolojik olarak uygunluğunu vurgulamaktadır. Bu sebeple, elde edilen KYT-PLA doku iskelelerinin, kemik doku mühendisliği uygulamaları için yüzeyde 3 boyutlu doku iskeleleri üretimi ve kök hücrelerinin farklılaşmasına yol göstereceği yönünde büyük bir potansiyel teşkil ettiği öngörülmektedir.

Anahtar Sözcükler: Biyomimetik, Kemik doku mühendisliği, Kök hücreler.

TABLE OF CONTENTS

ACKNOWLEDGMENTS iii
ABSTRACT iv
ÖZET v
LIST OF FIGURES ix
LIST OF TABLES xi
LIST OF SYMBOLS xii
LIST OF ABBREVIATIONS xiii
1. INTRODUCTION 1
1.1 Motivation 1
1.2 Objectives 4
1.3 Outline 4
2. BACKGROUND 5
2.1 Bone 5
2.1.1 Bone structure 5
2.1.2 Bone Repair 9
2.2 Bone Tissue Engineering 9
2.3 Polymeric Scaffolds in Bone Tissue Engineering 11
2.4 Stem Cells 12
3. MATERIALS AND METHODS 14
3.1 Preperation of Bone Surface Mimicked Scaffolds 14
3.2 Synthesis of Bone Surface Mimicked Scaffolds 15
3.3 Surface Characterization of Bone, PDMS and PLA Scaffolds 16
3.3.1 Scanning Electron Microscopy (SEM) 16
3.3.2 Contact Angle Measurements 17
3.3.3 Fourier Transform Infrared Spectroscopy (FTIR) 17
3.4 Atomic Force Microscopy (AFM) 18
3.5 In-vitro Degredation Studies 18
3.6 Drug Loading and Release 19
3.7 Cell Studies 19

3.7.1 Isolation and Culture of Human Bone Marrow Mesenchymal Stem Cells . . . 19
3.7.2 Cell Viability . . . 20
3.7.3 Osteogenic Differentiation . . . 20
3.7.4 Immunofluorescence Staining . . . 21
3.7.5 Statistical Analysis . . . 21
4. RESULTS . . . 22
4.1 Characterization of BSM Scaffolds . . . 22
4.1.1 Optimization of PLA Fabrication . . . 23
4.1.2 Fabrication of Multiple PDMS Molds Using Same Bone Surface 24
4.1.3 Fabrication of Multiple PLA Scaffolds Using Same Bone and PDMS Molds . . . 26
4.2 Wettability of the PLA Scaffolds . . . 28
4.3 FTIR Analysis . . . 29
4.4 Surface Roughness of Plain and BSM PLA Scaffolds . . . 30
4.5 Degradation of PLA Scaffolds . . . 31
4.6 Drug Release Study . . . 31
4.7 Cell Studies . . . 32
4.7.1 Cell Viability . . . 32
4.7.2 Differentiation Capacity of hBM MSCs on Plain and Bone Surface Mimicked PLA Scaffolds . . . 34
5. DISCUSSION . . . 38
5.1 SEM Analysis . . . 38
5.2 Wettability of PLA Scaffolds . . . 40
5.3 FTIR Analysis . . . 40
5.4 Surface Roughness of Plain and BSM PLA Scaffolds . . . 41
5.5 In-vitro Degradation of PLA Scaffolds . . . 41
5.6 Drug Release Studies . . . 42
5.7 Cell Studies . . . 42
5.8 Future Studies . . . 43
APPENDIX A. CALIBRATION CURVE . . . 45
APPENDIX B. Flow Cytometric Analysis . . . 46

B.1 Adipogenic and Osteogenic Differentiation 47
REFERENCES 48

LIST OF FIGURES

Figure 2.1	Position of bone cells	6
Figure 2.2	Crystal structure of HA mineral	7
Figure 2.3	Micro to nano structure of bone	8
Figure 2.4	Fracture bridging by callus	10
Figure 2.5	Application of stem cells in bone tissue engineering	12
Figure 3.1	Xenograft cleaning process	15
Figure 3.2	Experimental steps of the preperation of BSM and drug loaded BSM PLA scaffolds	16
Figure 3.3	Optical images of A) bone, B) PDMS and C) PLA	16
Figure 4.1	SEM images of A) bone surface topography, B) negative template of the same bone using PDMS as a mold, C) positive template of the same bone using 10% PLA (g polymer/ml $CHCI_3$) at RT	22
Figure 4.2	Mimicking process comparison of 2.5%, 5.0% and 10.0% BSM PLA scaffolds	23
Figure 4.3	The effect of casting time to mimicking procedure	24
Figure 4.4	SEM images of 1^{st} to 5^{th} PDMS negative templates and bone surface	25
Figure 4.5	SEM images of 1^{st} to 5^{th} PLA as positive replica	26
Figure 4.6	SEM images of 10^{th}, 15^{th} and 20^{th} PLA as positive replica	27
Figure 4.7	Contact angle images of plain and BSM PLA scaffolds	28
Figure 4.8	FTIR spectra of A) Drug(diclofenac), B) PLA, C) Drug loaded PLA	29
Figure 4.9	AFM topography images of a) 10% plain PLA b) 10% bone surface mimicked PLA	31
Figure 4.10	Weight loss of plain and BSM PLA scaffolds in PBS solution at 37 °C	32
Figure 4.11	Degradation morphology of plain PLA	32
Figure 4.12	Degradation morphology of BSM PLA Scaffolds	33
Figure 4.13	Diclofenac release from plain and BSM PLA scaffolds	34

Figure 4.14	Viability of human bone marrow mesenchymal stem cells	34
Figure 4.15	Differentiation capacity of human bone marrow mesenchymal stem cells on plain and BSM PLA labeled with anti-collagen type I antibody	35
Figure 4.16	Differentiation capacity of human bone marrow mesenchymal stem cells on plain and BSM PLA labeled with anti-osteocalcin antibody	36
Figure 4.17	Differentiation capacity of human bone marrow mesenchymal stem cells on plain and BSM PLA labeled with anti-osteonectin antibody	37
Figure A.1	Diclofenac calibration curve	45
Figure B.1	Flow cytometric analyses	46
Figure B.2	Conformation of MSCs differentiation	47

LIST OF TABLES

Table 4.1	Contact angles of plain PLA, 2.5 to 10.0% bone surface mimicked PLA	28
Table 4.2	FTIR peaks band assignment of PLA	30
Table 4.3	FTIR peaks band assignment of Diclofenac	30

LIST OF SYMBOLS

W	Description of Weight

LIST OF ABBREVIATIONS

PDMS	Polydimethylsiloxane
BSM	Bone Surface Mimicked
PLA	Polylactic Acid
SEM	Scanning Electron Microscopy
PBS	Phosphate Buffer Saline
hBM MSCs	Human Bone Marrow Mesenchymal Stem Cells
BMSCs	Bone Marrow Mesenchymal Stem Cells
HA	Hydroxyapatite
PGA	Poly(glycolic Acid)
PLGA	Polylactic-co-glycolic Acid
ESCs	Embryonic Stem Cells
BM	Bone Marrow
UCB	Umbilical Cord Blood
MSCs	Mesenchymal Stem Cells
ADSCs	Adipose Tissue-Derived Stem Cells
MDSCs	Muscle Derived Stem Cells
DPSCs	Dental Pulp Stem Cells
RT	Room Temperature
FTIR	Fourier Transform Infrared Spectroscopy
AFM	Atomic Force Microscopy
DMF	Dimethyformamide
FBS	Fetal Bovine Serum
ELISA	Enzyme-linked Immunosorbent Assay
DAPI	4',6-Diamidino-2-Phenylindole
FITC	Fluorescein Isothiocyanate

1. INTRODUCTION

1.1 Motivation

The term biomimicry (biomimetic) refers to mimic nature, to design solution inspired by nature and it aims to resolve human health problems [1]. There are lots of biomimetic examples that directly imitate the mechanical properties, structure color, optical properties, self-cleaning properties from the natural sources to the practical life [2, 3, 4, 5, 6]. In some studies, leaf templates, butterfly wings, water strider legs were directly mimicked by using polymers to obtain large area of hydrophobic surfaces [7]. By the inspiration of biomimicry research, including the knowledge of effectiveness of surface topography on bone repair and regeneration, one is motivated to investigate further the surface topography of artificial bone substitutes for promising application in bone tissue engineering. Therefore, mimicking the bone surface is a good approach that has been established in bone tissue engineering field.

In order to treat bone defects like osteogenesis imperfecta, osteoarthritis, osteomyelitis, and osteoporosis where bone cannot function properly, bone repair and in some cases bone replacement is required [8]. These bone defects could be large size that are really challenging for orthopedicians. First approach to treat such bone defects is autograft which is gold standard technique and it is obtained from patient's own bone marrow. Second approach is using allograft which is obtained from same species' bone marrow. Both techniques have several disadvantages like second-site surgery, donor incompatibility and limitations of available bone tissue [9]. According to Blom et al. study, allografts also have some problems such as infection, antigenicity and cost [10]. The third one is xenograft, supplied from one species and transplanted to another species, which also have same limitations as allografts have [11]. In consequence, bone tissue engineering approach has been enhanced to defeat such limitation of bone tissue loss. Due to the high energy trauma, multiple surgery, disease, and developmental deformity after implantation, designing of implant and patients care after implantation are notably important in order to prevent those outcomes [11].

To reduce all of these problems and side effects, bone tissue engineering aims to combine tissue scaffolds with cells and this combination will help to repair and regeneration of bone tissue. Therefore, bone tissue engineering is a concept which is able to enhance new therapeutic treatments for bone tissue loss and diminish the healing and recovery time day by day [11, 12, 13, 14]. The applicable scaffolds should assure the following properties which are interconnected porous structure, optimized surface topography for cell attachment and migration, biocompatible, biodegradable [11, 12]. Thus, different types of scaffolds are used in order to replace bone such as ceramics, metals and alloys, natural polymers like collagen and chitin, biodegradable and bioresorbable polymers [15, 16, 17, 18, 19]. Biodegradable polymers have a certain advantages such as controlling the surface properties, cellular adhesion and cellular response [20]. The chemical properties of biodegradable polymers allow hydrolytic degradation through de-esterification [19]. Once degraded, the monomeric components of each polymer are removed by natural pathways. Highly regulated mechanism in order for removing monomeric components of lactic and glycolic acids already exists in the body. That is why biodegradable polymers are so preferable in order for drug delivery systems and bone tissue engineering applications [19]. The nature of the polylactic acid (PLA) is also allowed to load drug in its matrix scaffolds and PLA can locally release growth factors or antibiotics and enhance bone ingrowth to treat bone defects and even support wound healing. PLA degradation starts with water uptake and following with the ester bonds hydrolysis [19].

The most useful property of PLA is that it is not only being biocompatible and biodegradable but also degraded to non-toxic byproducts and having drug loading capacity. Drug loaded polymeric scaffolds may help to process of tissue repair and regeneration. Also, drug release profile can be controlled with respect to scaffolds' degradation profile [21]. One of drug used to treat arthritis disorders is diclofenac which is non-steroidal and anti-inflammatory and used in this thesis as a model drug [22]. Thus, it is so promising polymer for bone tissue engineering applications.

Stem cells are undifferentiated cells that are capable of long term self-renewal and differentiation into all cell types. In mammals, there are two types of stem cells which are embryonic stem cells and adult stem cells. Whereas embryonic stem cells have the potential to differentiate into cells of all of the three germ layers, adult stem

cells can differentiate into only certain types of cells [23]. Some of the adult stem cells, which are multipotent, that means they have the restricted ability to differentiate certain types of the cells are adipose-derived stem cells, mesenchymal stem cells and hematopoietic stem cells. Along with them, researches may produce stem cells having the pluripotency from non-pluriotent adult cells by inducing those adult cells, namely induced pluripotent stem cells. Mesenchymal stem cells can be found many adults tissues including adipose and bone marrow. Bone marrow mesenchymal stem cells (BMSCs) can be differentiated to osteoblasts, chondrocytes, and fibroblasts. Based on the environment that cells cultured, these cells can constitute to aimed tissue [24, 25, 26]. Thus, bone marrow mesenchymal stem cells are desired therapeutic cells for bone tissue regeneration and repair.

Briefly, to improve the surface topography of artificial bone substitutes, mimicking the bone surface is promising technique that has been established in bone tissue engineering field. Biomimicry of bone surface is very effective method to prepare the similar micro-environment for bone cells (i.e. osteoblasts) by mimicking the surface topography of bone.

1.2 Objectives

In this study, polylactic acid (PLA) was used as a biocompatible and biodegradable polymer to mimic bone surface topography. Then bone marrow mesenchymal stem cells differentiation was investigated on PLA scaffolds. In order to decrease the side effect of the implantation process, a model drug, diclofenac, was loaded on the PLA and its releasing profile was investigated, as well. The main objectives of this study are:

- To mimic the surface topography and roughness of bone by using the biodegradable polymers
- To characterize the mimicked surfaces of bone physically and chemically
- To investigate the degradation of polymers and also release profile of the loaded model drug
- To examine the cell response on the bone surface mimicked biodegradable PLA scaffolds.

1.3 Outline

The thesis is presented as follows: In chapter 2, background information about bone and its structure, approaches in bone repair and regeneration, bone tissue engineering are given. In chapter 3, the experimental procedures are explained. In chapter 4, the results are presented. In chapter 5, the discussion of the results and their implications are given.

2. BACKGROUND

2.1 Bone

In human physiology, bone provides support, movement and shape for the entire body as well as protection for some organs. Bone also plays an essential role for blood production, mineral storage and homeostasis, blood pH regulation, multiple progenitor cell (mesenchymal, hemopoietic) housing and also regulation of electrolytes concentration in blood [8, 27].

2.1.1 Bone structure

Bone is considered as a distinct organ formed by three essential components which are bone cells, bone minerals and bone matrix. Its organic substrate composes of abundantly collagen type I (approximately 40% of volume), its inorganic material is largely hydroxyapatite (approximately 45% of volume) and the water exists in the rest of the volume (approximately 15%). Most important properties are stiffness and strength of bone. Thus, this combination makes the bone's mechanical properties particular in terms of stiffness and tensile strength [8, 28].

Osteogenic precursor cells, osteoblasts, osteocytes, osteoclasts, bone lining cells and hemopoietic bone marrow cells are bone cell types which are originated from either hematopoietic stem cells or mesenchymal stem cells. For example, while osteoblasts, osteocytes and bone lining cells are derived from mesenchymal stem cells; osteoclasts are derived from hemopoietic stem cells. The position of bone cells is also different from each other. Osteoblasts, osteoclasts and bone lining cells are placed along the surface; but osteocytes are found at the inner site of bone (Figure 2.1) [29, 30].

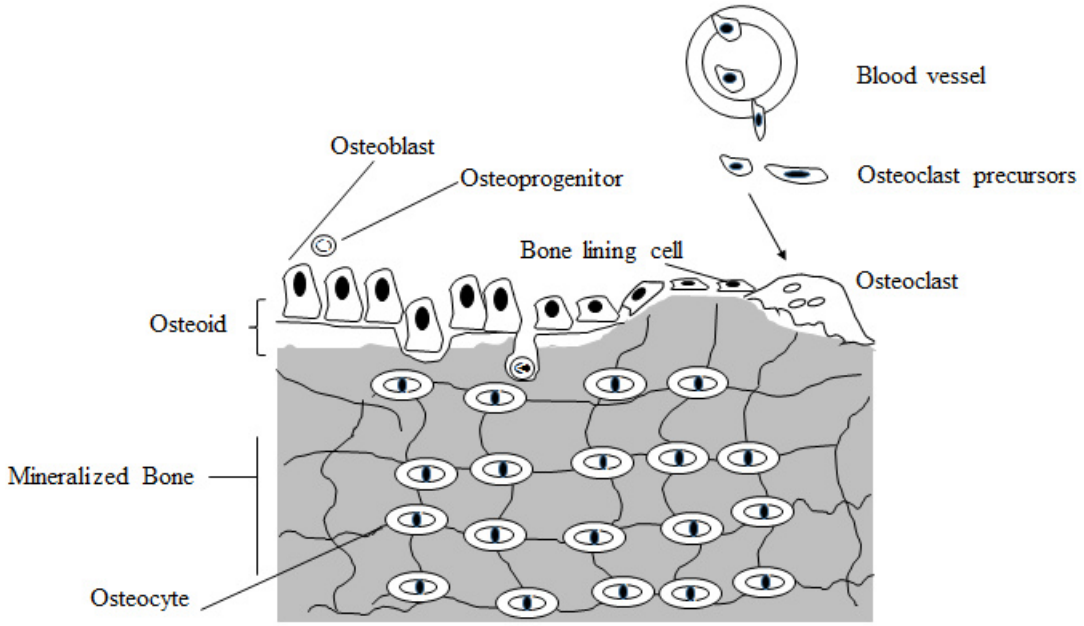

Figure 2.1 Position of bone cells [29].

Osteoblasts are responsible for bone formation and they participate in matrix development and calcification. Osteocytes are responsible for extracellular concentrations of calcium and phosphate. Also, they allow cell to cell interaction, ion and growth factor transportation with their extensions called canaliculi. Osteoclasts are responsible for bone resorption. They are able to break down organic and inorganic matrix of bone [30].

As it mentioned previously, 90% of extracellular matrix composed of both organic and inorganic components and the remaining 10% is bone cells and blood vessels [29]. Type I collagen whose polypeptide chain have the primary structure (Gly-X-Y) is the abundant organic component of bone. In this polypeptide chain, X and Y define as proline and hydroxyproline frequently. In addition, small amount of type III, type V, and type XII collagen are found in bone organic matrix [29, 31]. The inorganic component of bone is abundantly composed of calcium phosphate which is present in the form of hydroxyapatite (HA) as it is shown in Figure 2.2. It can be located at surface of bone or embedded in collagen fibrils. Hydroxyapatite provides strength and resistance to compression. The collagen fibers provide resistance to tensile forces.

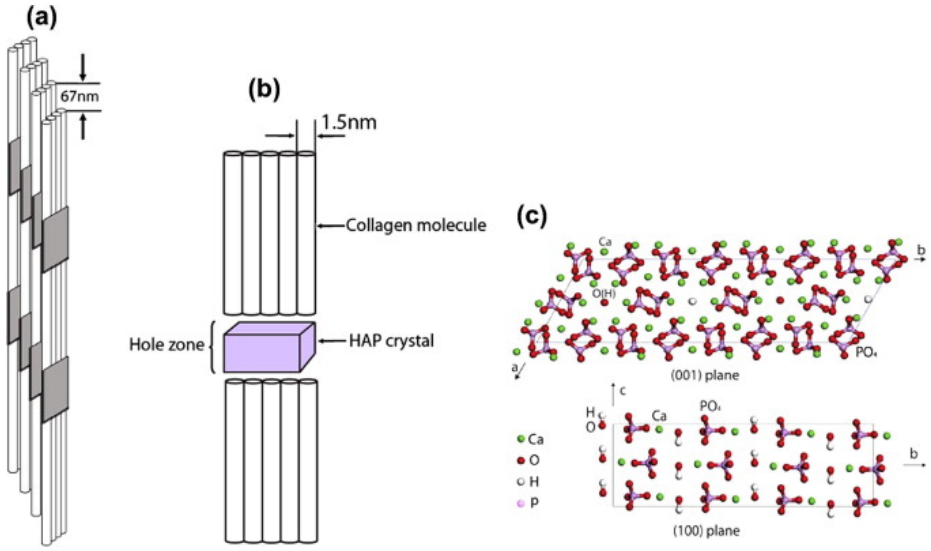

Figure 2.2 Crystal structure of HA mineral [32].

Bone structure can be divided in two parts as compact (cortical) and cancellous (spongy). Compact bone found on the surface of the bone is very dense and solid. Cancellous bone found in the interior of bones has a relatively porous structure. Function and location of the bone can be effect the relative amount of compact and cancellous bone [29]. Cortical and cancellous bone can contain woven or lamellar bone, as well [29]. Outer layer of cortical bone is coated with periosteum which is a fibrous connective tissue. Periosteum consists of closely packed osteons also called Haversian systems. Osteon is the basic structural unit of cortical bone formed by bundles of collagen fibers with bone minerals and bone cells embedded in. Each osteon has a central Haversian canal and it is containing blood vessels and nerves enveloped in bone tissue called lamellae. Lamellae are arranged by parallel alignment of collagen into those enveloped sheets. Cancellous bone contributes a space for bone marrow, where blood cells are produced, blood vessels and connective tissues exist. Hence, it supports bone functions and homeostasis. Hierarchical structural organization of bone is given in Figure 2.3 [33].

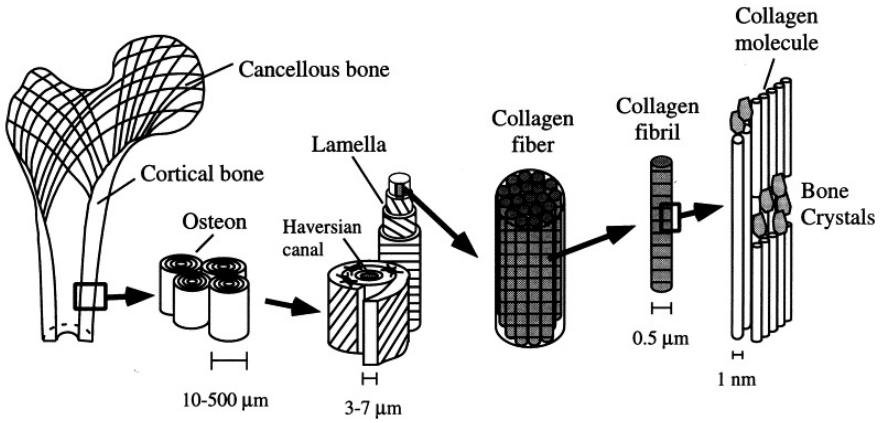

Figure 2.3 Micro to nano structure of bone [33].

Bone cellular activities, modeling and remodeling, take place on the bone surfaces where the only region available for them. That is why bone surfaces have exclusive importance for cellular activities with regards to mechanical and nonmechanical features. Bone surfaces are grouped as periosteal and endosteal surfaces. The periosteum covers the outer of the bone. Periosteum is formed by the 4.4% of the total bone surface. The endosteal surface is categorized as intracortical surface (Haversian canals), endocortical surface and trabecular surface. The endosteal surface is formed by 30.4% intracortical surface, 4.4% endocortical surface and 60.8% trabecular surface of total bone surface. Undifferentiated cells take place on the periosteal surface and during bone growth, new bones are adding onto the outer surface. As a result, the cross-sectional area of long bone increases. Bone formation is decreased to tolerable level during adulthood period. When bone is fractured, the periosteum plays an essential role in bone repair pocess. During remodeling, the skeleton renews itself on the endosteal surface, constantly. It is done to sustain biomechanical strength and supply metabolic needs. The bone remodeling includes three important steps which are resporption, formation and quiescence (resting state) [29]. Remodeling period can be varied in different parts of the human body. For example, the alveolar bone is more metabolically active than other types of bone which leads to fast remodeling than other bones [34].

2.1.2 Bone Repair

As it is mentioned in previous section, bone repair and remodeling include both periosteum and endosteum surfaces. Facture healing is dynamic process which involves cell growth, differentiation factors, hormones, extracellular matrix. All of them regulate cellular events that end with bone healing. Fracture healing results in three continuous steps which are inflammatory stage, reparative stage and remodeling stage. Reparative phase includes intramembranous ossification, chondrogenesis, and endochondral ossification [31]. In inflammation stage, also called immediate reaction, bleeding is occurred and vasodilation and leukocytes migration have been started. Therefore, cell division is increased. During this process, hematoma formation begins between the bonds in which migrated cells and bioactive agents exist. Angiogenesis and tissue granulation is also obtained in this stage [35]. The illustration of bone healing as the bridging by callus is shown in Figure 2.4. Both cell proliferation and differentiation and callus formation are occurred in reparative phase. In following process, fractured bone is healed by mineralization. This new bone tissue goes through remodeling phase. In this phase, bone resorption and formation progress in order to give the bone its original shape, function and physical properties [35].

2.2 Bone Tissue Engineering

Tissue engineering can be defined as engineering and materials method that combine together with the biochemical and life sciences to improve or replace tissue functions [16]. Large area bone defects are challenging for orthopaedician and require orthopedic implants and mechanical requirements for load bearing conditions [14]. Traditional treatment methods like autografts or allografts end up with some limitations due to the bone defects' size and shape or unexpected bone resorption [14]. With the help of tissue engineering, the application of biological and engineering principles come together to restore function or to replace damaged or diseased tissues. When specialized to bone tissue engineering, the main purpose is to create bone formation

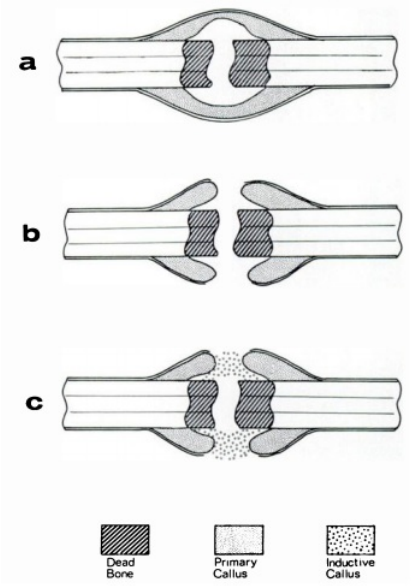

Figure 2.4 Fracture bridging by callus, a) involving of perioustum, b) primary callus response, c) bridging of callus with the formation of soft tissue [35].

and to achieve biomechanical properties of surrounding [14, 31]. In bone tissue engineering, bone healing and regeneration start with the series of cellular events which are stimulated by biological and mechanical factors. In order to sustain biological factors, osteoprogenitor cells capable of forming bone are required. For the mechanical factors, a suitable tissue substitutes, also called scaffolds, should be used [14, 31, 36]. Thus, osteocunductive properties of bone substitutes promote the bone repair response. Bone tissue engineering, for the purpose of this thesis, is the use of a scaffold to promote the formation of bone from the surrounding tissue or to act as a carrier or template for implanted bone cells.

A variety of materials such as metals, ceramics, polymers (natural and synthetic) and their combinations have been used for replacement and repair of bone tissues. Metals and ceramics have certain disadvantages like non degradability and limited processability. On the other hand, polymers have a lot of good properties, mainly flexibility and biodegradability, which are really promising for bone tissue engineering application. They can degrade by hydrolysis, cellular or enzymatic pathways. Its design and application can be effect bone healing and cellular response [37]. Hence, polymeric scaffolds are abundantly used for bone tissue engineering application.

To sum up, the fundamental concept behind bone tissue engineering is to uti-

lize the body's natural biological response to bone defect with the help of engineering principles. Ideal scaffolds should be able to present physiochemical biomimetic environment such as mechanical support, encouraging bone cell migration, producing nontoxic degradation products and promoting osteogenic differentiation [14, 36, 37].

2.3 Polymeric Scaffolds in Bone Tissue Engineering

Many types of polymers are used for bone tissue engineering application categorized as natural and synthetic polymers. Natural polymers like collagen and fibrils have possible advantage to support cellular response [37]. In spite of their biological recognition advantage, their mechanical properties and biodegradability are hard to control. In addition, the cost of natural polymers is high and its availability in market is limited. Besides, the advantages of synthetic polymers like poly(lactic acid) (PLA), poly(glycolic acid) (PGA), and their copolymers polylactic-co-glycolic acid (PLGA) are that their surface architecture, mechanical and degradation properties can be adjusted with respect to requirements of tissue defects [37].

The chemical properties of biodegradable polymers allow hydrolytic degradation and degradation products are removed by natural pathways. That is why biodegradable polymers are so preferable in order for drug delivery systems and bone tissue engineering applications [19]. The nature of the PLA is also allowed to load drug in its matrix scaffolds and PLA can locally release growth factors or antibiotics and enhance bone ingrowth to treat bone defects and even support wound healing. PLA degradation starts with water uptake and following with the ester bonds hydrolysis. There are many techniques to produce PLA scaffolds and most common techniques are solvent casting, phase inversion, fiber bonding, melt based technologies, high pressure based methods, freeze drying, and rapid prototyping [38]. Solvent casting method is the most common and simple techniques among them. Basically, polymer is dissolved with organic solvent to produce a solution. Then this polymer-solvent solution is subjected to solvent removal by either evaporation or extraction process [39].

For bone tissue engineering application, surface topography of polymeric scaf-

folds should provide cell attachment and proliferation. Scaffolds' pores should be interconnected to allow cell migration and transportation of nutrients and waste. For the biomechanical point of view, mechanical properties are also necessary for cellular behavior [37, 40]. Therefore, synthetic polymers are promising for cellular response and scaffolds for tissue engineering.

2.4 Stem Cells

Stem cells are undifferentiated cells that are capable of long term self-renewal and differentiation into all cell types. In mammals, there are two types of stem cells which are embryonic stem cells and adult stem cells. Along with them, researches may produce stem cells having the pluripotency from non-pluriotent adult cells by inducing those adult cells, namely induced pluripotent stem cells [41]. Whereas embryonic stem cells have the potential to differentiate into cells of all of the three germ layers, adult stem cells can differentiate into only certain types of cells [23]. Due to the lack of donor tissue, various stem cells have been considered as potential appliance for the field of bone tissue engineering. These unique properties make them an attractive cell source for bone tissue engineering applications as it shown in Figure 2.5.

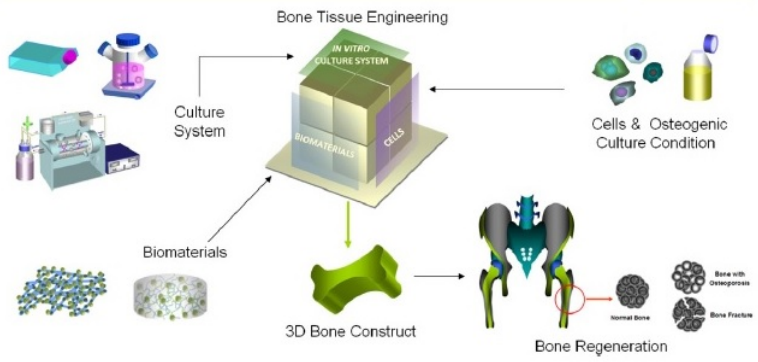

Figure 2.5 Application of stem cells in bone tissue engineering [42].

In order to form bone cells, various types of stem cells are used such as embryonic stem cells (ESCs), bone marrow (BM)-derived or umbilical cord blood (UCB)-derived mesenchymal stem cells (MSCs), adipose tissue-derived stem cells (ADSCs), muscle-derived stem cells (MDSCs) and dental pulp stem cells (DPSCs). Bone marrow stroma contains bone marrow mesenchymal stem cells (BMSCs) and it is capable to form bone; so that BMSCs are used for bone regeneration. For therapeutic reasons, BMSCs can be isolated and then expanded in culture to sustain available amount of cell mass [43]. In addition to that, appropriate cell culture environment like collagen substrate, growth factor supplementation can help to sustain cell differentiation potential (Figure 2.5) [41, 43]. Therefore, BMSCs have advantages when used for bone tissue engineering. By using the master scaffolds (with molecular, structural and mechanical properties designed to mimic bone) and suitable microenvironment, the osteogenic capacity of stem cells to treat bone defects can be tested [23, 41, 43].

3. MATERIALS AND METHODS

3.1 Preperation of Bone Surface Mimicked Scaffolds

Bovine femur was used to prepare bone surface mimicked (BSM) scaffolds and supplied from a local butcher. Bone was cut into small pieces using a bone saw and cleaned by xenograft cleaning process (Figure 3.1) [44]. Xenograft cleaning process includes osmotic bath (ultrasonic bath), oxidative and alkaline process. To get rid of remaining cells and tissue on the bone, bone pieces were placed into the 10% NaCI solution for 24h. The first 20 minutes of this process was done in ultrasonic bath. The acetone bath was also applied in order to remove lipids or lipid groups. 3% H_2O_2 was used for the removal of immunologic structures. For the effectiveness of this step, the first and last 5 minutes were done in ultrasonic bath. This process inactivates the prions that are harmful for collagen and inorganic structure of bone. 2N NaOH was used and the first 15 minutes of this process was done in ultrasonic bath. By completing this cleaning procedure, cleaned bone pieces were obtained. As it is given in Figure 3.2, in the first part of the experiments, bone surface topography was mimicked by using those cleaned bones with Polydimethylsiloxane (PDMS) as a mold by soft lithography technique [45]. After obtaining the PDMS mold, polylactic acid (PLA) was poured onto this mold and the effect of PLA concentration (2.5-10% (w/v) in chloroform) and casting time (as evaporated-24h) were investigated on the mimicking procedure at room temperature (RT). Then, the bone surface mimicked PLA scaffolds obtained. In second part, in order to investigate in-vitro degradation and drug release, bone surface mimicked, drug (diclofenac, a non-steroidal anti-inflammatory drug) loaded PLA scaffolds were prepared. In the last part of the thesis, osteogenic differentiation of bone marrow mesenchymal stem cells was investigated.

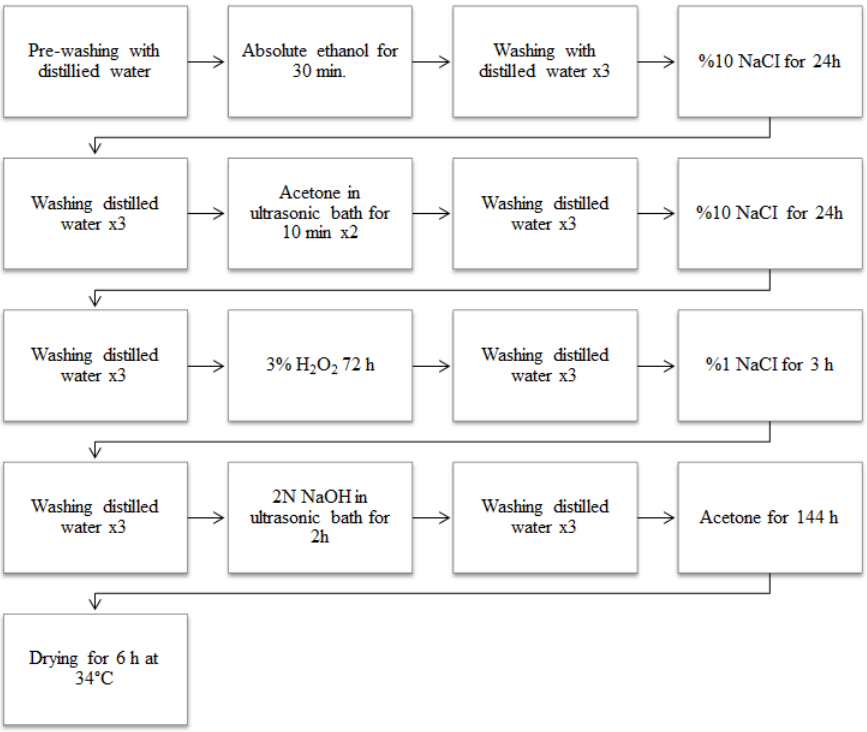

Figure 3.1 Xenograft cleaning process [44].

3.2 Synthesis of Bone Surface Mimicked Scaffolds

Bovine femur surface topography was mimicked by using bovine femur with PDMS (Sylgard 184; Dow Corning, Midland, MI) by soft lithography technique [45]. At mass ratio 10:1 PDMS was prepared by mixing silicon elastomer with curing agent and the cup was placed in a dessicator to degas (allow gasses to rise out) till all the gasses were removed. Then the PDMS was poured on bone surface and placed in an incubator for 4h at 70 °C. The PDMS was used as a mold in order to transfer the surface topography of the bone to a biodegradable polymer polylactic acid (PLA) (intrinsic viscosity, 1.8 dl/g, 221.000 g/mol MW). First, PLA was dissolved in chloroform ($CHCI_3$) at 60 °C and poured onto this mold and then the effect of PLA concentration (2.5-10% (w/v) in $CHCI_3$) and casting time (as evaporated-24h) were investigated at RT. After that process, the surface topography of bone was transferred to the PLA scaffold. The optical images of bone, PDMS and PLA were given in Figure 3.3.

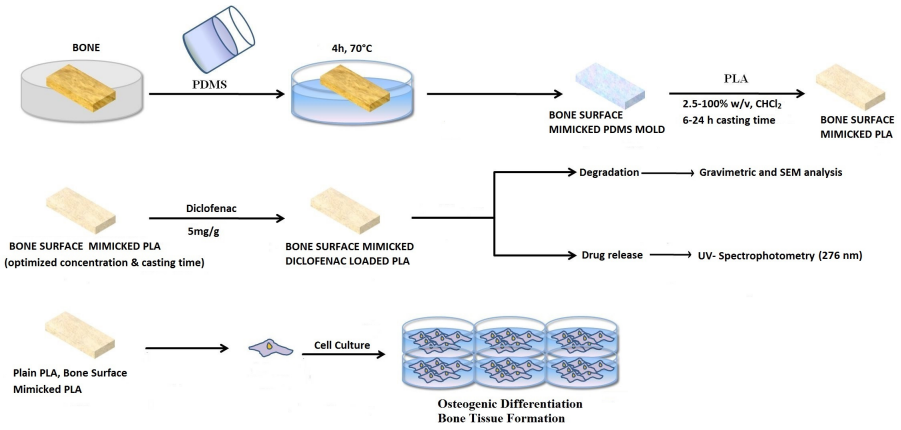

Figure 3.2 Experimental steps of the preperation of BSM and drug loaded BSM PLA scaffolds.

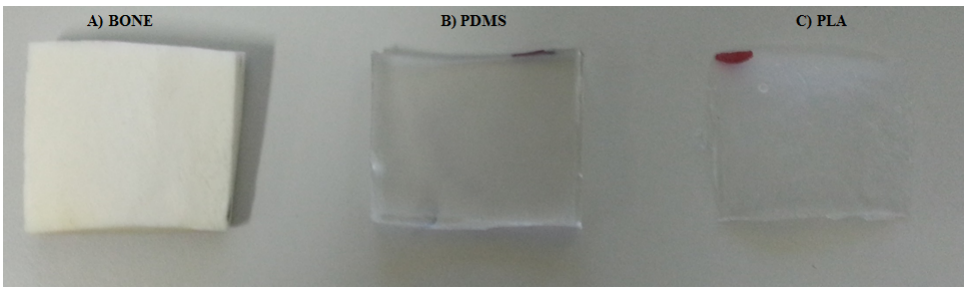

Figure 3.3 Optical images of A) bone, B) PDMS and C) PLA.

3.3 Surface Characterization of Bone, PDMS and PLA Scaffolds

3.3.1 Scanning Electron Microscopy (SEM)

Surface topography of bovine femur, PDMS and PLA were examined using scanning electron microscopy (SEM) (Philips XL30 ESEMFEG/EDAX) at Bogazici University Research and Development Center Electron Microscopy and Microanalysis Unit. All surfaces were coated with thin layer of 50 nm gold and then SEM images were performed [46, 47]. Before scanning every piece of bone, the reference point was set to observe mimicking profile. SEM was used to determine if the PDMS surfaces

used as a mold were successful to mimick the bone surface. The reference point on the bone surface and the mirror image of the same reference point on PDMS surface were compared using SEM images. The PLA surfaces were also investigated using SEM to determine the best mimicking concentration (2.5-10% w/v PLA concentration) and casting time (as evaporated-24h) in the mimicking procedure.

3.3.2 Contact Angle Measurements

Surface contact angles of plain and BSM PLA with different concentrations (2.5-10% (w/v) in $CHCI_3$) was measured to get information in the hydrophilicity and hydrophobicity of the scaffolds. For this purpose, contact angle measurement device (DSA 100, Krüss GmbH, Germany) was used to measure the advancing contact angles of plain and 2.5%, 5.0% and 10.0% ((w/v) in $CHCI_3$) BSM PLA scaffolds. The contact angle measurements were performed at Bogazici University Chemical Engineering Department. The initial drop volume was 10μl and the dosing rate was set at 10μl/min for each measurement. All measurement was performed at RT [48].

3.3.3 Fourier Transform Infrared Spectroscopy (FTIR)

FTIR spectra were recorded over the range of 4000 to 400 cm^{-1} with 32 scans in order to investigate the chemical compositions of PLA, drug loaded PLA and drug [49]. The FTIR measurement were perfomed at Hacettepe University Department of Chemistry.

3.3.4 Atomic Force Microscopy (AFM)

The plain and bone surfaced mimicked PLA scaffolds surface roughness was characterized by using AFM. First of all plain and BSM PLA scaffolds was cut in a small pieces (1 cm^2) and stuck on metal disk (1 cm outer diameter) by double sided cellophane tape. Surface topography of the BSM and plain PLA surface was investigated in non-contact mode of atomic force microscopy. The measurements were performed at Hacettepe University Department of Chemistry [50].

3.4 In-vitro Degredation Studies

In order to investigate the degradation profile by means of weight loss and surface erosion, in vitro degradation study was performed. Plain and BSM PLA were cut in 1 cm^2 and each one was placed in 2ml PBS (pH=7.4, Sigma Aldrich) solution at 37 °C. Every week, PLA scaffold samples were taken out, dried at 37 °C and weighted again. By using equation 3.1, the weight loss was calculated [51, 52]. Surface topography of degraded PLA scaffolds at initial time and 2^{nd}, 4^{th} and 8^{th} weeks were examined by SEM [46, 47]. Each result was the average of five parallel measurements, expressed as mean ± standard deviation.

$$WeightLoss(\%) = [(W_0 - W_t) \div W_0] \times 100\% \tag{3.1}$$

3.5 Drug Loading and Release

PLA was dissolved in $CHCl_3$ at a concentration of 10% and a model drug diclofenac (5mg/g polymer)(Sigma Aldrich, United State) was added to the solution until the homogeneous mixture was obtained [21]. The drug release measurments were performed at Bogazici University Institute of Biomedical Engineering Biomaterials Laboratory. Then drug/polymer solution poured into PDMS and drug loaded bone surface mimicked PLA scaffolds were casted. Also, plain drug loaded PLA was synthesized using the same procedure. Drug release profile of both scaffolds was measured by UV-Spectrophotometry (Nanodrop 2000c Spectrophotometer, Thermo Scientific, USA). The wavelength was selected as 276 nm for diclofenac maximum absorbance. For the drug release studies, scaffolds were cut as 1 cm^2, then they were put into 2 ml phosphate buffer saline (PBS) solution and the drug release measurements were performed at 2^{nd}, 4^{th} days and 1, 2, 4, 8 and 16 weeks at 37 °C. Each result was the average of six parallel measurements, expressed as mean ± standard deviation.Calibration curve for diclofenac was given in Appendix A.

3.6 Cell Studies

3.6.1 Isolation and Culture of Human Bone Marrow Mesenchymal Stem Cells

Human bone marrow mesenchymal stem cells (hBM MSCs) were isolated and grown in culture at the PEDI-STEM Stem Cell Laboratory of Hacettepe University using frozen marrow samples obtained from a healthy bone marrow transplant donor and ethical committee project number for the research was GO14/41. In order to confirm that the isolated cells used in the experiments were bone marrow mesenchymal stem cells (BM MSCs), the flow cytometry analysis were done. Details and results were given in Apendix B.

hBM MSCs at passage 1 (frozen sample) were cultured in Dimethyformamide10

(DMF10) medium consisting of low-glucose-Dulbecco's Modified Eagle's Medium and MCDB (Invitrogen, Carlsbad, CA), 10% fetal bovine serum (FBS; Invitrogen), and 1% penicillin/streptomycin (Biochrom) at 37 °C in a humidified incubator (5% CO_2) for 3 days before the first medium change. The medium was subsequently changed twice a week. At 80-85% confluence, cells were trypsinized (Gibco Invitrogen), and cell viability was assessed by trypan blue dye exclusion. BM MSCs at passage 3 ($2x10^4$ cells per 24-well plate) were seeded on plain and BSM PLA surfaces. Cell seeding and growth were checked with phase contrast microscope [53].

3.6.2 Cell Viability

Cell viability tests were carried out with hBM MSCs that were seeded on plain and BSM PLA scaffolds at the density of $2x10^4$ cells per well that were incubated in 24-well tissue culture plates previously coated with biopolymers. Cultures were carried on for 3 days. At least 3 replicates were studied for each condition. After 72 h of incubation, the cell metabolic activity was assessed using water-soluble tetrazolium-based assay [10% WST-1, 4'-[3-(4-iodophenyl)-2-(4-nitrophenyl)-2H-5-tetrazolio]-1,3-benzenedisulfonate] for 2.5 hours. 100 mL of medium for each condition was transferred into enzyme-linked immunosorbent assay (ELISA) microplates (96-wells plates) for spectrophotometric measurement. The absorbance of the solutions were measured spectrophotometrically at 450 nm [53].

3.6.3 Osteogenic Differentiation

hBM MSCs were seeded on the plain and BSM PLA scaffolds and osteogenic differentiation was induced 72 h after seeding using StemPro Osteo Basal Medium, Stem Pro Osteogenesis Supplements (Invitrogen) and 1% penicillin/streptomycin (Lonza) at 37 °C in a humidified incubator (5% CO_2). Cell growth was checked with phase contrast microscope during 10 days of culture. All images were captured with a CKX41

microscope (Olympus, Tokyo, Japan) [53].

3.6.4 Immunofluorescence Staining

Non-osteogenically and osteogenically induced hBM MSCs at day-7 were fixed with ice cold aceton for 10 minutes at room temperature then permeabilized with PBS/Saphonin (0.5%, Sigma) and washed with PBS/Tween (0.05%, Fisher Scientific, Canada). 4′, 6-Diamidino-2-phenylindole (DAPI) (Sigma) stain was used for nucleus staining. Monoclonal anti-human collagen type I antibody (Abcam and Santa Cruz Biotechnology) and fluorescein isothiocyanate (FITC) conjugated secondary antibody were used for receptor staining. Similar protocols were performed for osteocalcin and osteonectin staining for non-osteogenically and osteogenically induced cells at day 10, then examined under a DM 4000 photolight microscope (Leica, Wetzlar, Germany) [53].

3.6.5 Statistical Analysis

Statistical significance was evaluated based on Student t-test; value of $p<0.05$ was considered significant [53].

4. RESULTS

4.1 Characterization of BSM Scaffolds

Surface topography of bone, its negative template PDMS, and positive template PLA (10% w/v polymer in $CHCl_3$) were given in Figure 4.1. These SEM images were taken by using a single bone, PDMS as a mold and 10% PLA as bone positive template. Four different regions of bone were examined and then their SEM images were performed to compare with PDMS negative template and 10% PLA positive template by the same regions. The four different region of bone in Figure 4.1 part A and negative template of bone in Figure 4.1 part B were compared with PLA surface topography in Figure 4.1 part C. Therefore, bone surface topography was successfully mimicked by PLA.

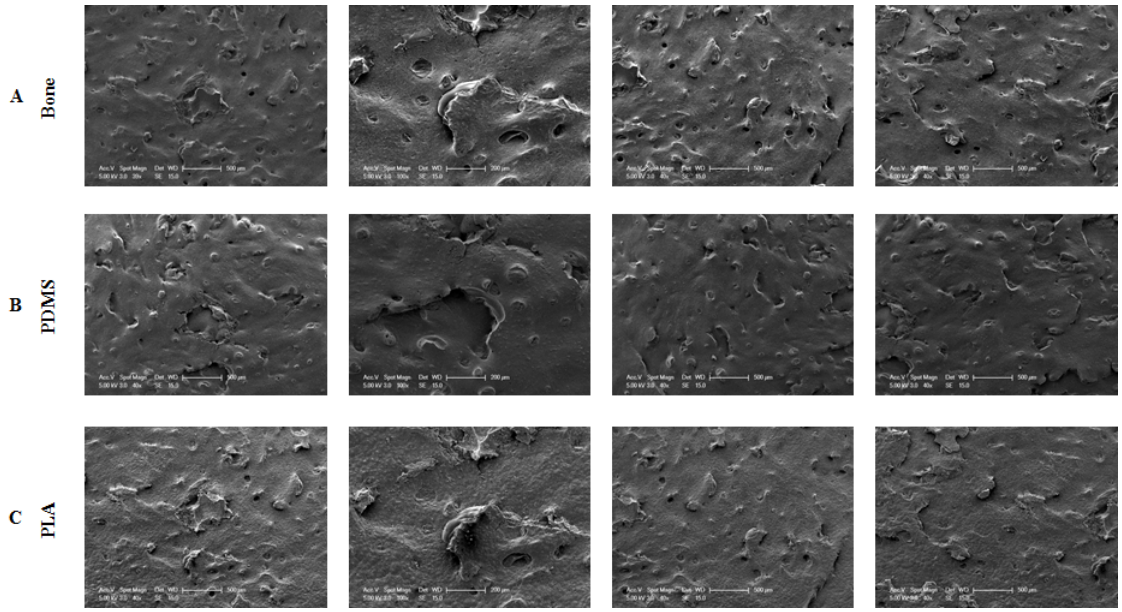

Figure 4.1 SEM images of A) bone surface topography; B) negative template of the same bone using PDMS as a mold, C) positive template of the same bone using 10% PLA (g polymer/ml $CHCl_3$) at RT.

4.1.1 Optimization of PLA Fabrication

Bone surface mimicked PLA scaffolds were prepared with different concentrations (2.5-10% w/v in g polymer/ml $CHCI_3$) in order to decide which PLA concentration had a better mimicking potential. For the comparison of 2.5%, 5.0% and 10.0% bone surface mimicked PLA scaffolds, SEM analysis was performed and surface topography images were given in Figure 4.2. It can be clearly implied that 10.0% PLA concentration has the best mimicked PLA scaffold characteristic. After deciding the optimum concentration, casting time of 10% PLA on PDMS mold was examined. 10% PLA solution was casted on PDMS with three different casting time which were the time of chloroform evoporation, 6 h and 24 h. The effect of casting time in surface topography was given in Figure 4.3. It can be implied that 24 h casting time resulted the best mimicked PLA scaffold characteristic.

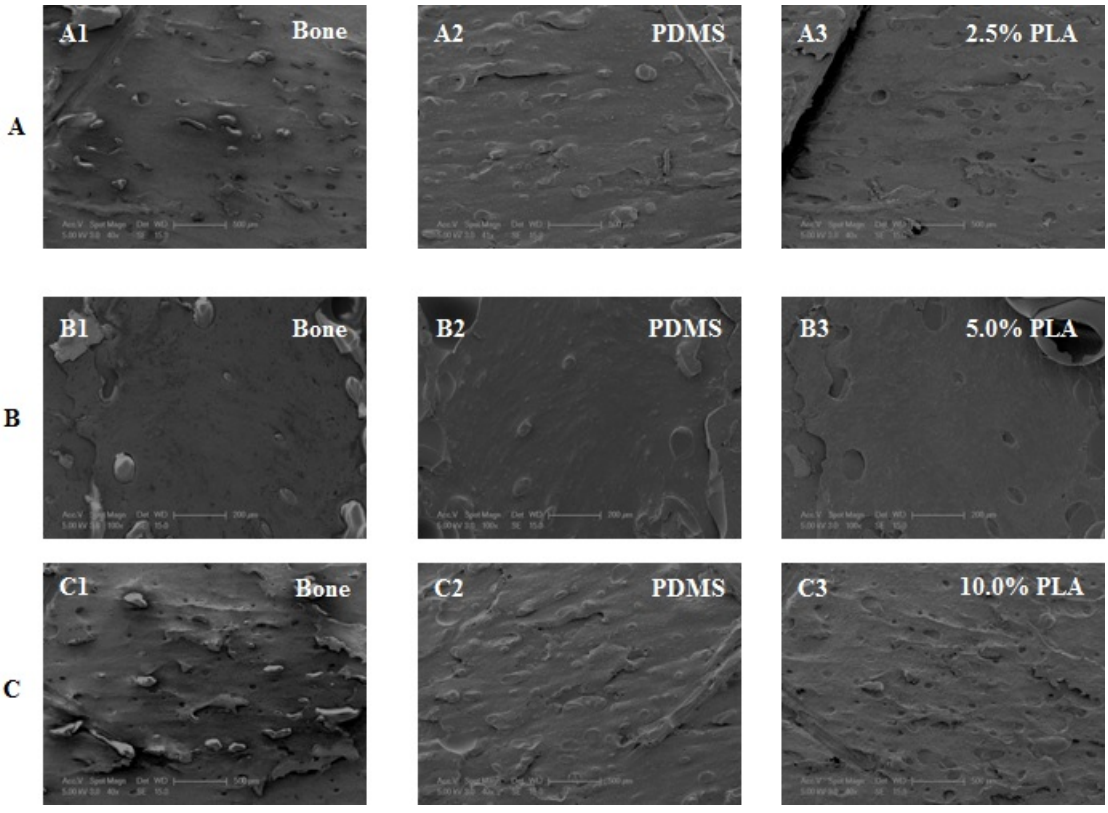

Figure 4.2 Mimicking process comparison of BSM PLA scaffolds prepared by different PLA concentration A3) 2.5%, B3) 5.0% and C3) 10.0% (w/v polymer in g polymer/ml $CHCI_3$) BSM PLA scaffolds.

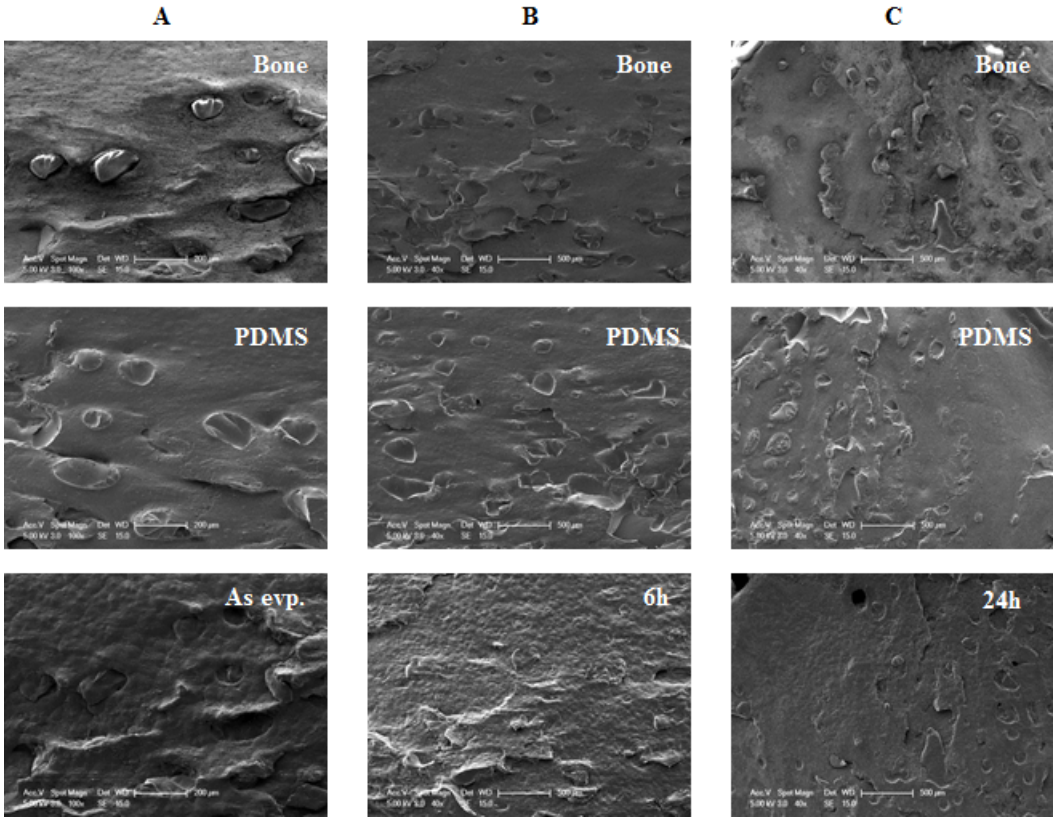

Figure 4.3 The effect of casting time to mimicking procedure at RT. SEM images of different casting time by using 10% PLA as A) the time of chloroform evoporation (as evp.); B) 6h; C) 24h.

4.1.2 Fabrication of Multiple PDMS Molds Using Same Bone Surface

In order to examine the effectiveness of mimicking procedure, same bone surface was used for synthesizing PDMS mold for 5 times. Surface topography of three different regions of same bone and 5 PDMS negative templates were shown in Figure 4.4 that there were no significant differences between 1^{st} and 5^{th} PDMS molds in terms of surface topography of bone.

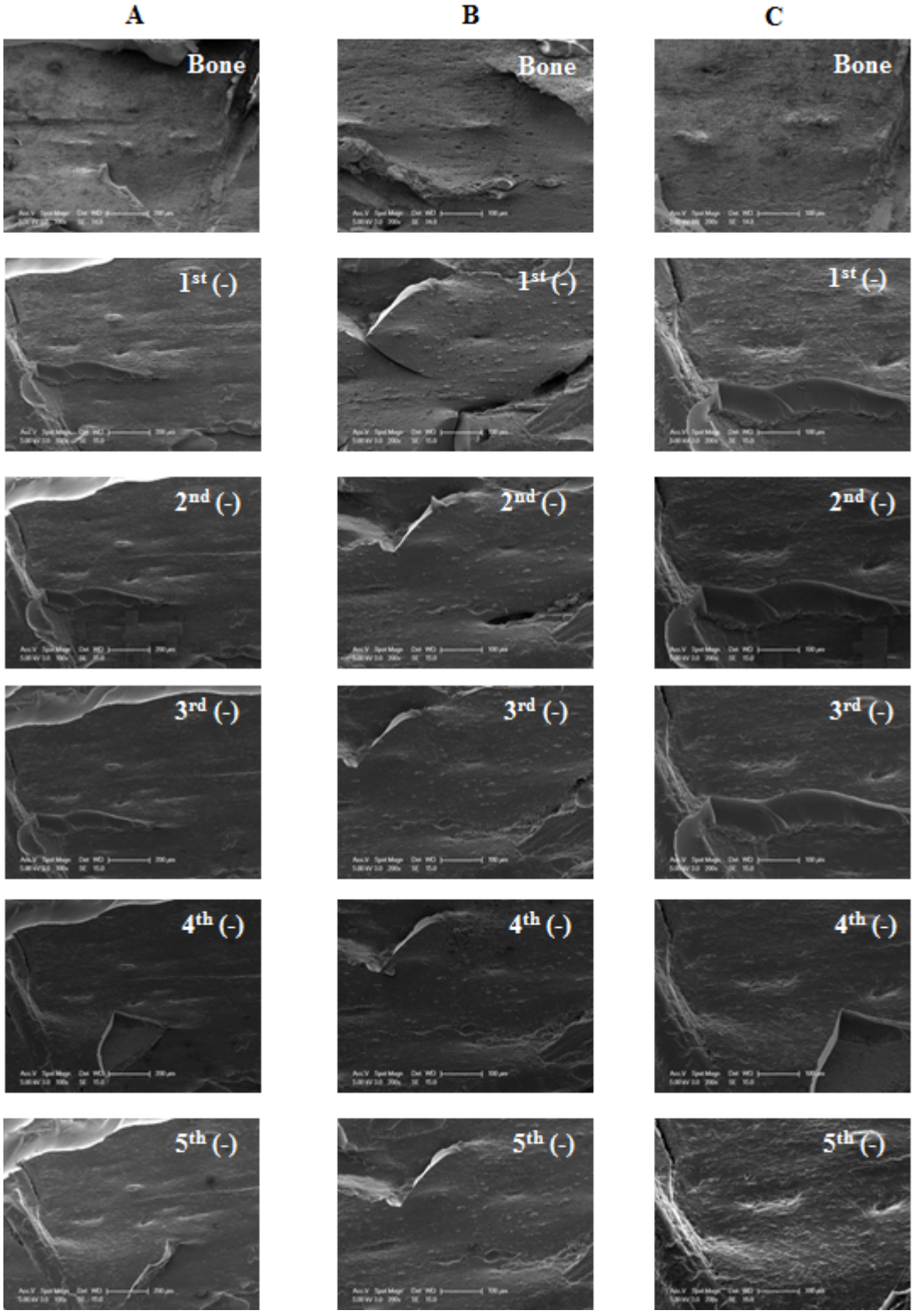

Figure 4.4 SEM images of 1^{st} to 5^{th} PDMS $(10:1)$ negative templates and bone surface. A) Area1, B) Area2 and C) Area3.

4.1.3 Fabrication of Multiple PLA Scaffolds Using Same Bone and PDMS Molds

Each 5 PDMS molds which were imaged in Figure 4.4 were used 20 times to prepare bone surface mimicked PLA scaffolds. Similar topography was observed from each set by using SEM. Surface topography images of 1^{st} and 5^{th} PLA scaffolds were given in Figure 4.5 and surface topography images of 10^{th}, 15^{th}, 20^{th} PLA scaffolds were given in Figure 4.6.

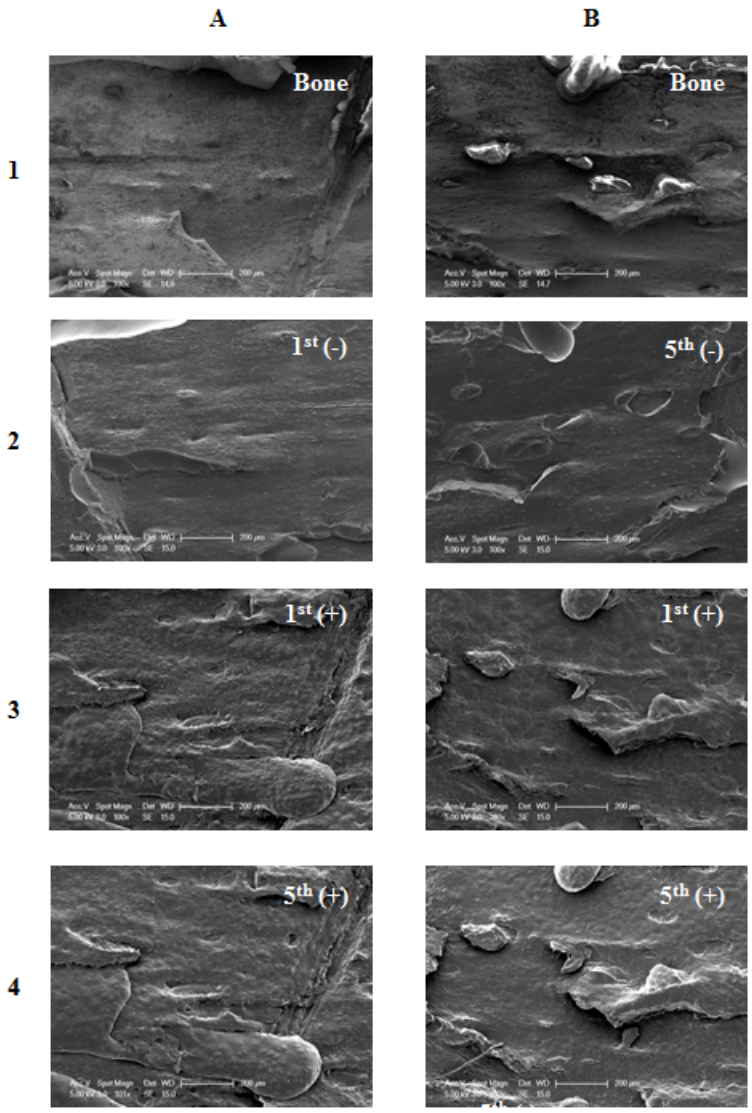

Figure 4.5 SEM images of two different region of same bone surface A-1) and B-1), 1^{st} to 5^{th}PDMS as negative replica of same bone A-1) 1^{st} PDMS replica B-2) 5^{th} PDMS, A-3) 1^{st} PLA as positive replica from 1^{st} PDMS replica, B-3) 1^{st} PLA as positive replica from 5^{th} PDMS replica, A-4) 5^{th} PLA as positive replica from 1^{st} PDMS replica, B-4) 5^{th} PLA as positive replica from 5^{th} PDMS replica.

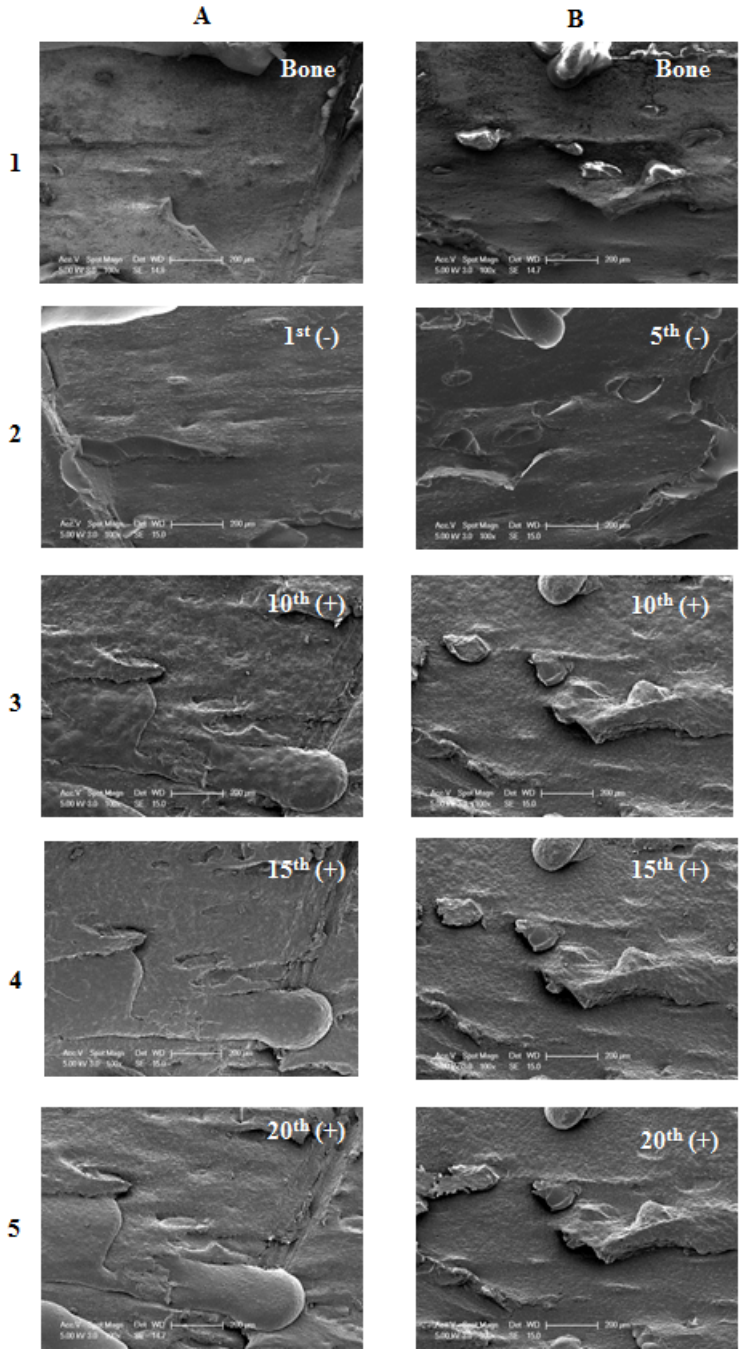

Figure 4.6 SEM images of two diffrent region of same bone surface A-1) and B-1), 1^{st} to 5^{th} PDMS as negative replica of same bone A-2) 1^{st} PDMS replica B-2) 5^{th} PDMS, A-3) 10^{th} PLA as positive replica from 1^{st} PDMS replica, B-3) 10^{th} PLA as positive replica from 5^{th} PDMS replica, A-4) 15^{th} PLA as positive replica from 1^{st} PDMS replica, B-4) 15^{th} PLA as positive replica from 5^{th} PDMS replica and A-5) 20^{th} PLA as positive replica from 1^{st} PDMS replica, B-5) 20^{th} PLA as positive replica from 5^{th} PDMS replica.

4.2 Wettability of the PLA Scaffolds

The water contact angles of plain and with different PLA concentrations (2.5-10.0% w/v in g polymer/ml $CHCI_3$) were shown in Table 4.1, and their contact angle images were shown in Figure 4.7. Water contact angle of plain PLA scaffold was lower than bone surface mimicked PLA scaffolds prepared with different concentrations. Hydrophobicity of PLA scaffold was increased as the concentration of bone surface mimicked PLA was increased from 65.88° ± 8.32 to 113.18° ± 9.68 from the 10% plain PLA to 10% BSM PLA scaffolds, respectively.

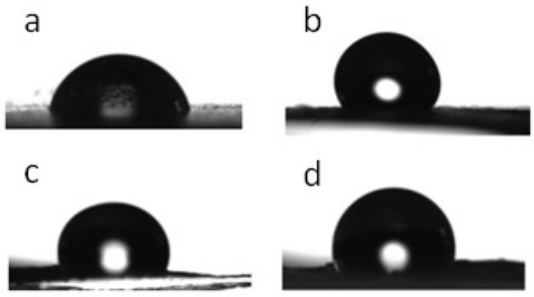

Figure 4.7 Contact angle images of plain and BSM PLA scaffolds a) plain PLA, b) 10% PLA, c) 5% PLA, d) 2.5% PLA.

Table 4.1
Contact angles of plain PLA, 2.5 to 10.0% bone surface mimicked PLA.

Samples	Contact Angle (°)
10.0% Plain PLA	65.88 ± 8.32
2.5% BSM PLA	76.90 ± 13.07
5.0% BSM PLA	93.49 ± 13.02
10.0% BSM PLA	113.18 ± 9.68

4.3 FTIR Analysis

The FTIR spectra of drug (diclofenac sodium) having the molecular formula $C_{14}H_{10}CI_2NNaO_2$, plain PLA having the molecular formula $(C_3H_4O_2)_n$ and drug loaded PLA were given in Figure 4.8. The IR spectra of diclofenac sodium exhibited distinctive peaks at 3386 cm^{-1}, 573 cm^{-1} and 745 cm^{-1} because of NH stretching of the secondary amine, $-C = O$ stretching of the carboxyl ion and beacuse of $C - Cl$ stretching, respectively [54]. The characteristic band of PLA was at 1747 cm^{-1} which corresponds to $-C = O$ ester group. The peaks at 2995 cm^{-1}, 1455 cm^{-1}, 1364 cm^{-1}, 1180 cm^{-1}, 1128 cm^{-1}, 1080 cm^{-1}, 1043 cm^{-1} and 871 cm^{-1} correspond to $-CH-$ stretch, $-CH-$ deformation (including sym and asym bend), $-C-O-$ stretch and $-C-C-$ stretch, respectively [55]. Both diclofenac sodium and PLA characteristic peaks were given in Figure 4.8.C as drug loaded PLA IR spectra. PLA and diclofenac peaks band assignments were given in Table 4.2 and 4.3, respectively.

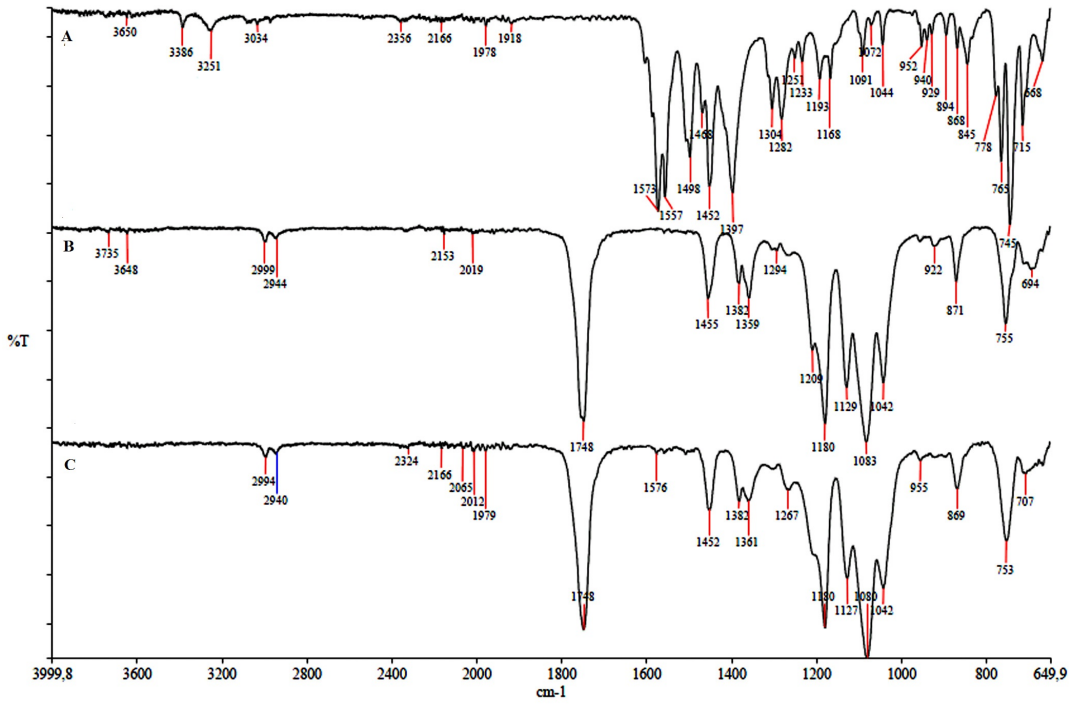

Figure 4.8 FTIR spectra of A) Drug(diclofenac), B) PLA, C) Drug loaded PLA

Table 4.2
FTIR peaks band assignment of PLA.

Chemical Bonds	FTIR Spectrum Peaks (cm^{-1})
-CH- stretch	2997.6, 2985
-C=O ester	1759.2
-CH- deformation (including sym and asym bend)	1456.3, 1383, 1368
-C-O- stretch	1269, 1186.3, 1134.6, 1091.8, 1045.5
-C-C- stretch	878

Table 4.3
FTIR peaks band assignment of Diclofenac.

Chemical Bonds	FTIR Spectrum Peaks (cm^{-1})
Asymmetric O=C-O^-	1575
C-N	1282, 1305
Aromatic C-Cl	745
Overtones (weak bonds)	1665 to 2000
Metallic salt Na^-	1452
Aromatic C-C	1604, 1469

4.4 Surface Roughness of Plain and BSM PLA Scaffolds

AFM images of plain PLA and bone surface mimicked PLA scaffolds were given in Figure 4.9. According to the AFM images, the plain PLA scaffold had a smooth surface while the bone surface mimicked PLA scaffolds have possed a rough surface. Roughness value of plain PLA is 1.70 nm and BSM PLA is 6.48 nm. Bone surface mimicked PLA surface was more rough than plain PLA surface in nanoscale.

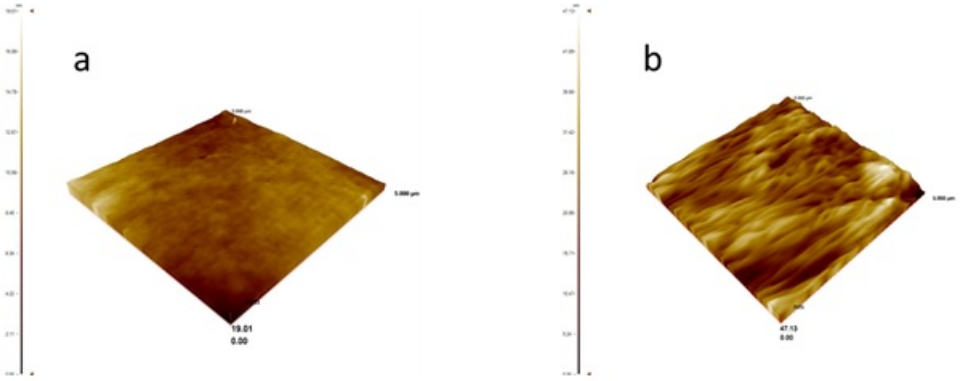

Figure 4.9 AFM topography images of a) 10% plain PLA b) 10% bone surface mimicked PLA.

4.5 Degradation of PLA Scaffolds

In vitro degradation of plain and BSM PLA scaffolds were evaluated by weight loss determination in the PBS medium for 9 weeks at 37 °C. The weight loss of plain and BSM PLA as a function of the degradation time was given in Figure 4.10. Plain and BSM PLA scaffolds have shown small degradation rate and degradation rate was stable during the week 3^{rd} and 7^{th}. Morphological change due to degradation were identified by SEM analysis. Plain and BSM PLA scaffolds surface morphology during the degradation were given in Figure 4.11 and Figures 4.12, repectively. Small morphological changes could be observed from both scaffolds. According to student t-test analysis, p value was equal to 0.007 which meant that the results were statistically significant.

4.6 Drug Release Study

Drug release from drug loaded plain and drug loaded BSM PLA scaffolds in PBS at 37 °C along 35 days was shown in Figure 4.13. A similar behavior was observed in both scaffolds, a fast initial release, almost linearly up to 7 days. Drug release has almost stopped after 1^{st} week. The amount of released drug is 48.6 μg for plain PLA and 7.4 μg for BSM PLA in two weeks.

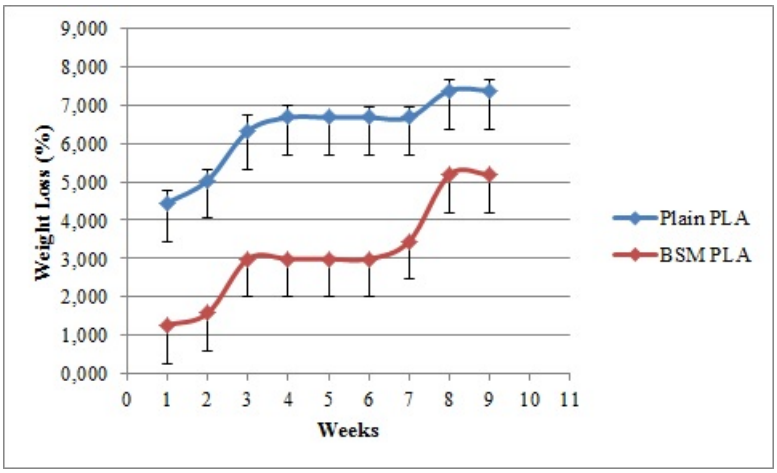

Figure 4.10 Weight loss of plain and BSM PLA scaffolds in PBS solution at 37 °C.

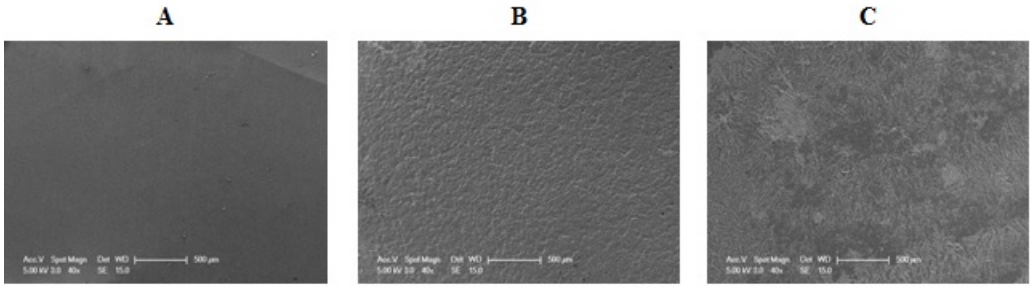

Figure 4.11 Degradation morphology of plain PLA from different region of scaffolds; A) initial, B) 2^{nd} week and 4^{th} week.

4.7 Cell Studies

4.7.1 Cell Viability

Cell viability is one of the important parameters to evaluate a particular material is biocompatible and/or suitable for bone tissue engineering [56]. Cell viability tests were carried out with hBM MSCs on plain and bone surface mimicked PLA scaffolds using water-soluble tetrazolium-based assay [10% WST-1, 4-[3-(4-iodophenyl)-2-(4-nitrophenyl)-2H-5-tetrazolio]-1,3-benzenedisulfonate] for assessing the cell metabolic activity. Cell viability of hBM MSCs on control (glass surface used as a control), plain

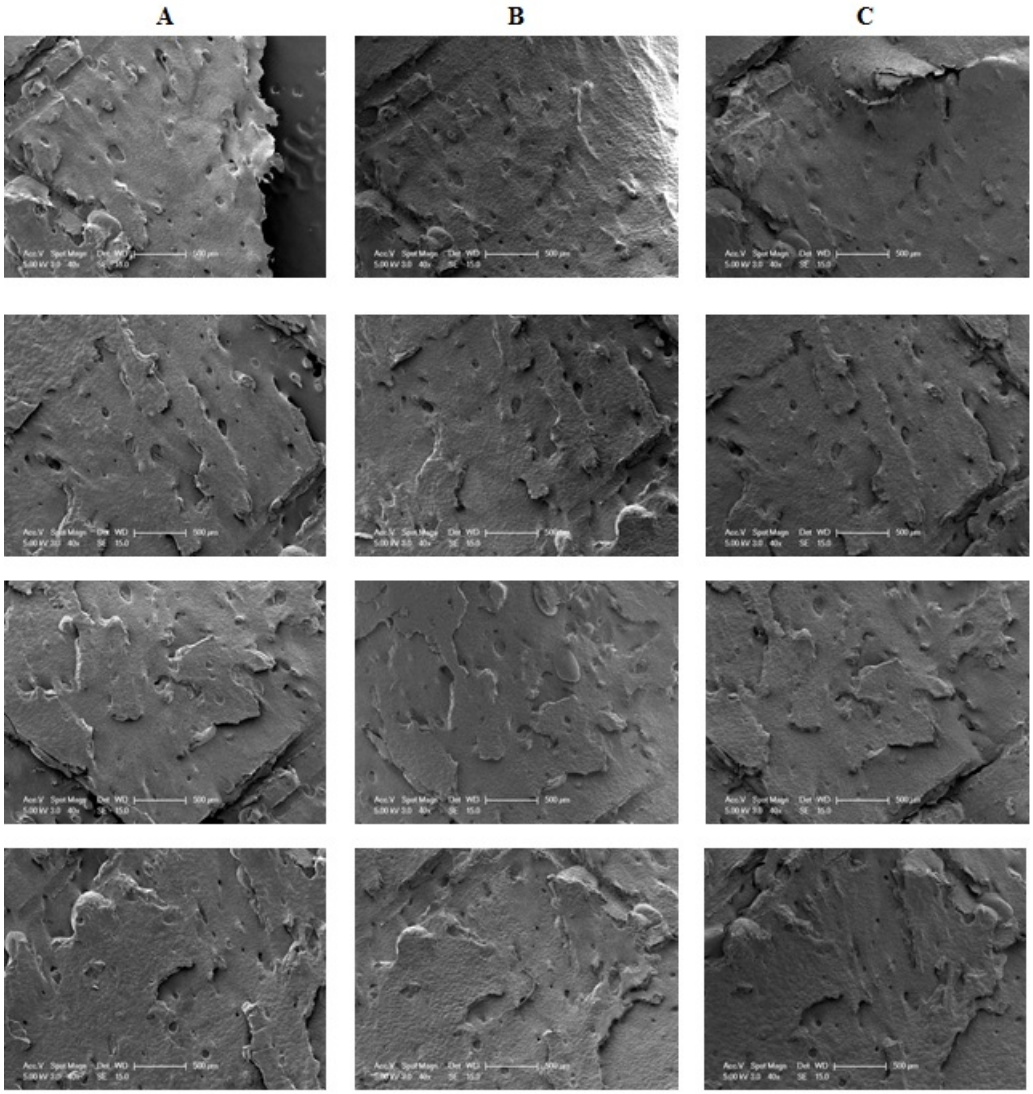

Figure 4.12 Degradation morphology of BSM PLA from four different region of scaffolds; A) initial, B) 2^{nd} week and 4^{th} week.

and bone surface mimicked PLA scaffolds were found to be 80.20 ± 6.695; 82.70 ± 6.281 and 83.90 ± 5.537, respectively (Figure 4.14). According to these data, highest viability were measured on bone surface mimicked PLA scaffolds.

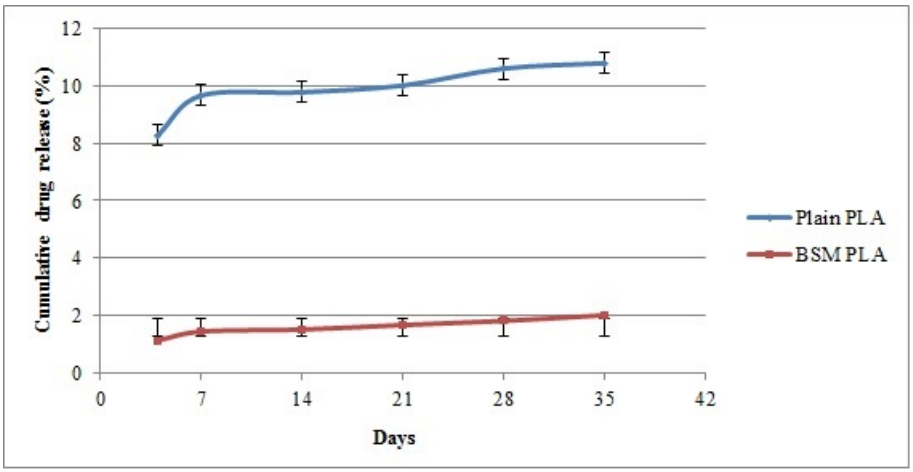

Figure 4.13 Diclofenac release from plain and BSM PLA scaffolds in PBS (pH 7.4) at 37 °C.

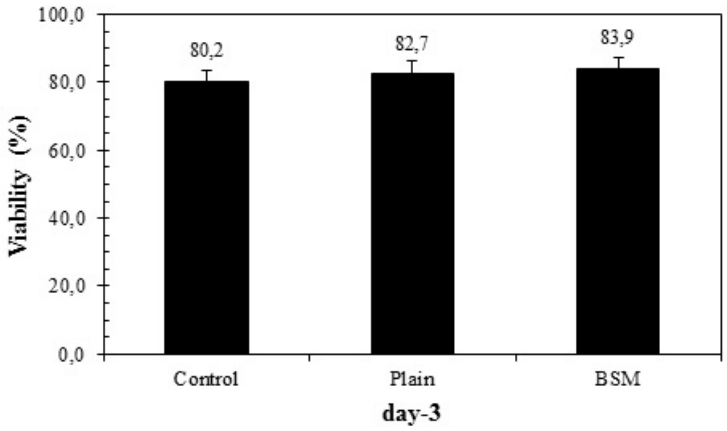

Figure 4.14 Viability of human bone marrow mesenchymal stem cells on control (glass surface), plain and bone surface mimicked PLA scaffolds.

4.7.2 Differentiation Capacity of hBM MSCs on Plain and Bone Surface Mimicked PLA Scaffolds

Differentiation capacity of human bone marrow mesenchymal stem cells on plain and bone surface mimicked PLA scaffolds investigated in non-osteogenically and osteogenically induced hBM MSCs at day-7 and 10. 4',6-Diamidino-2-phenylindole (DAPI) stain was used for nucleus staining. Monoclonal anti-human collagen type I antibody and FITC conjugated secondary antibody were used for receptor staining at day 7. Similar protocols were performed for osteocalcin and osteonectin staining

for non-osteogenically and osteogenically induced cells at day 10. Immunofluorescent images of collagen I, osteocalsin and osteonectin were shown in Figure 4.15, 4.16, 4.17, respectively.

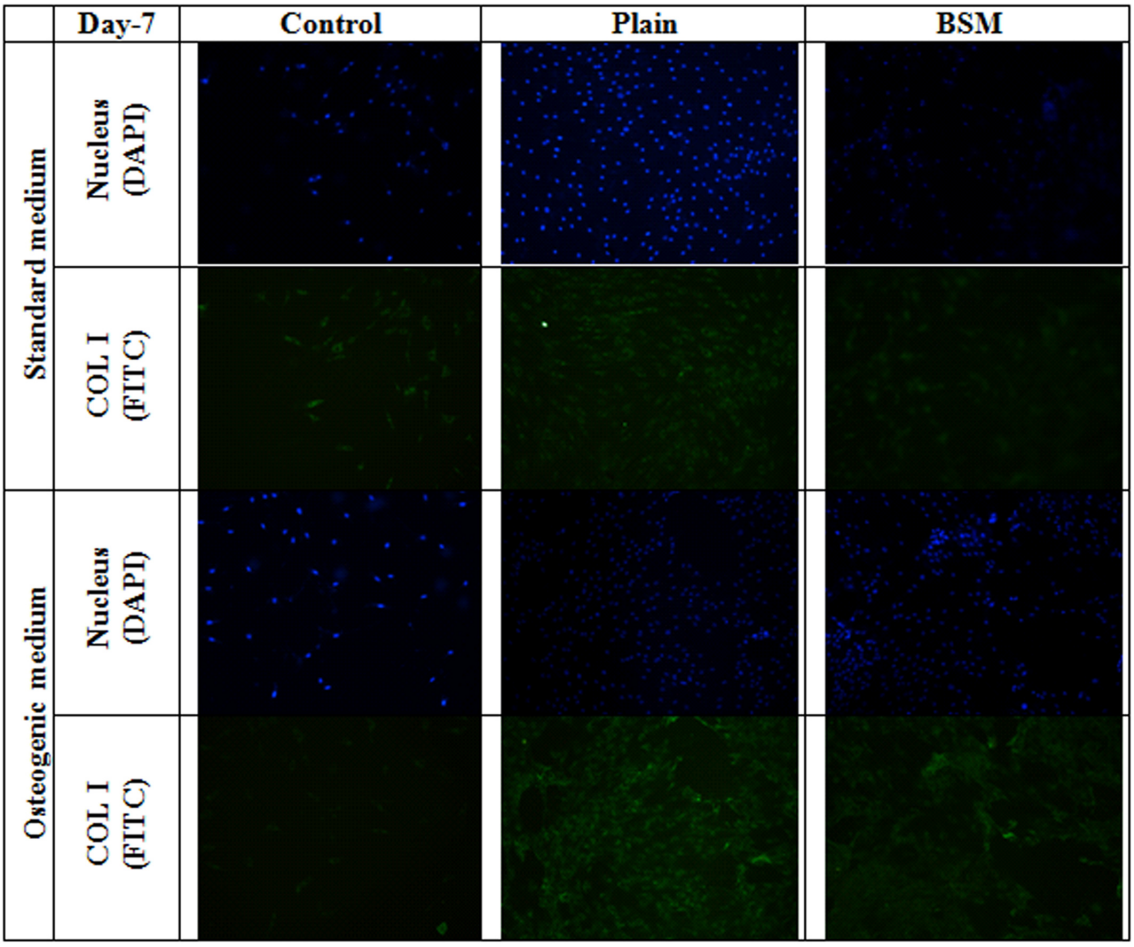

Figure 4.15 Differentiation capacity of human bone marrow mesenchymal stem cells on plain and BSM PLA labeled with anti-collagen type I antibody. Immunofluorescent images of hBM MSCs primed for 4 days and then differentiated for 7 days in the absence of a polymeric scaffolds (control, a-d); on the plain PLA (e-h); and on the bone surface mimicked PLA (i-l). magnification x 100.

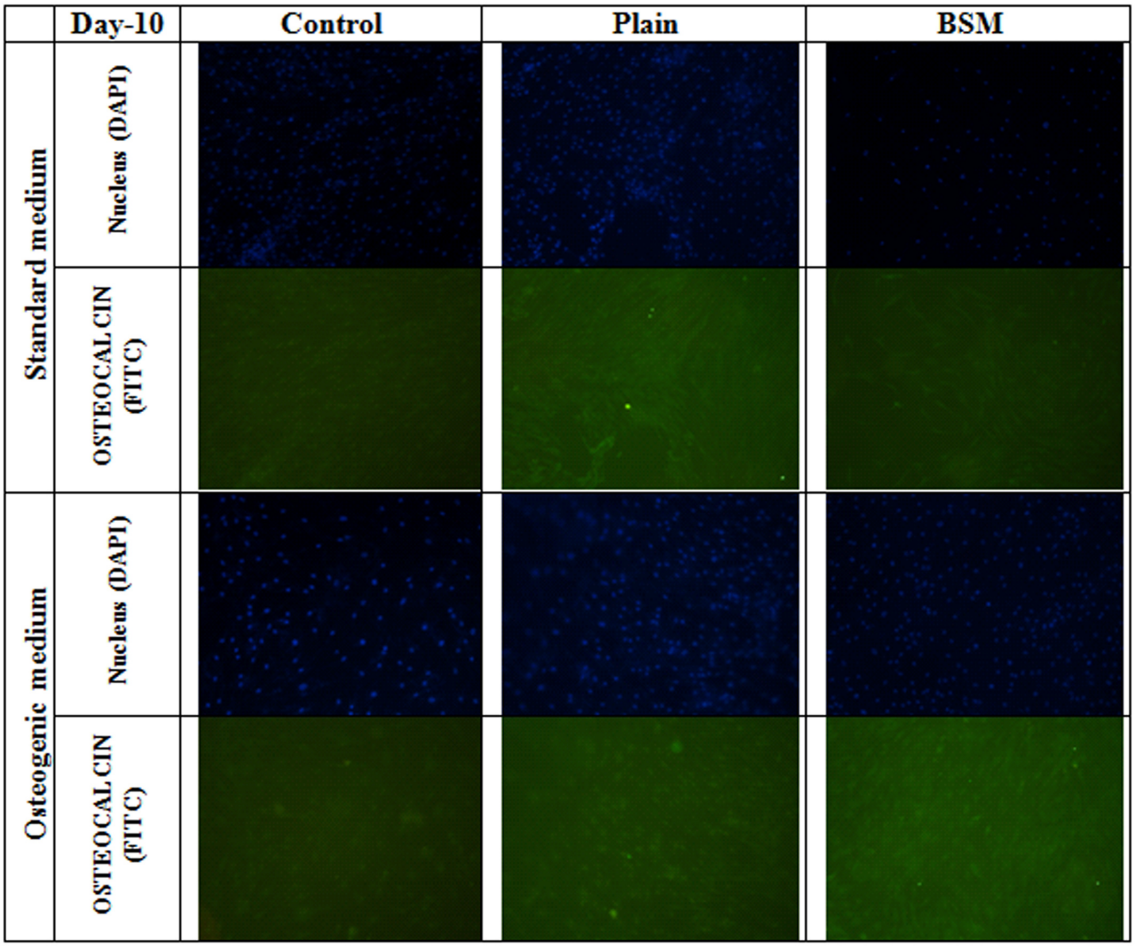

Figure 4.16 Differentiation capacity of human bone marrow mesenchymal stem cells on plain and BSM PLA labeled with anti-osteocalcin antibody. Immunofluorescent images of hBM MSCs primed for 4 days and then differentiated for 10 days in the absence of a polymeric scaffolds (control, a-d); on the plain PLA (e-h); and on the bone surface mimicked PLA (i-l). magnification x 100.

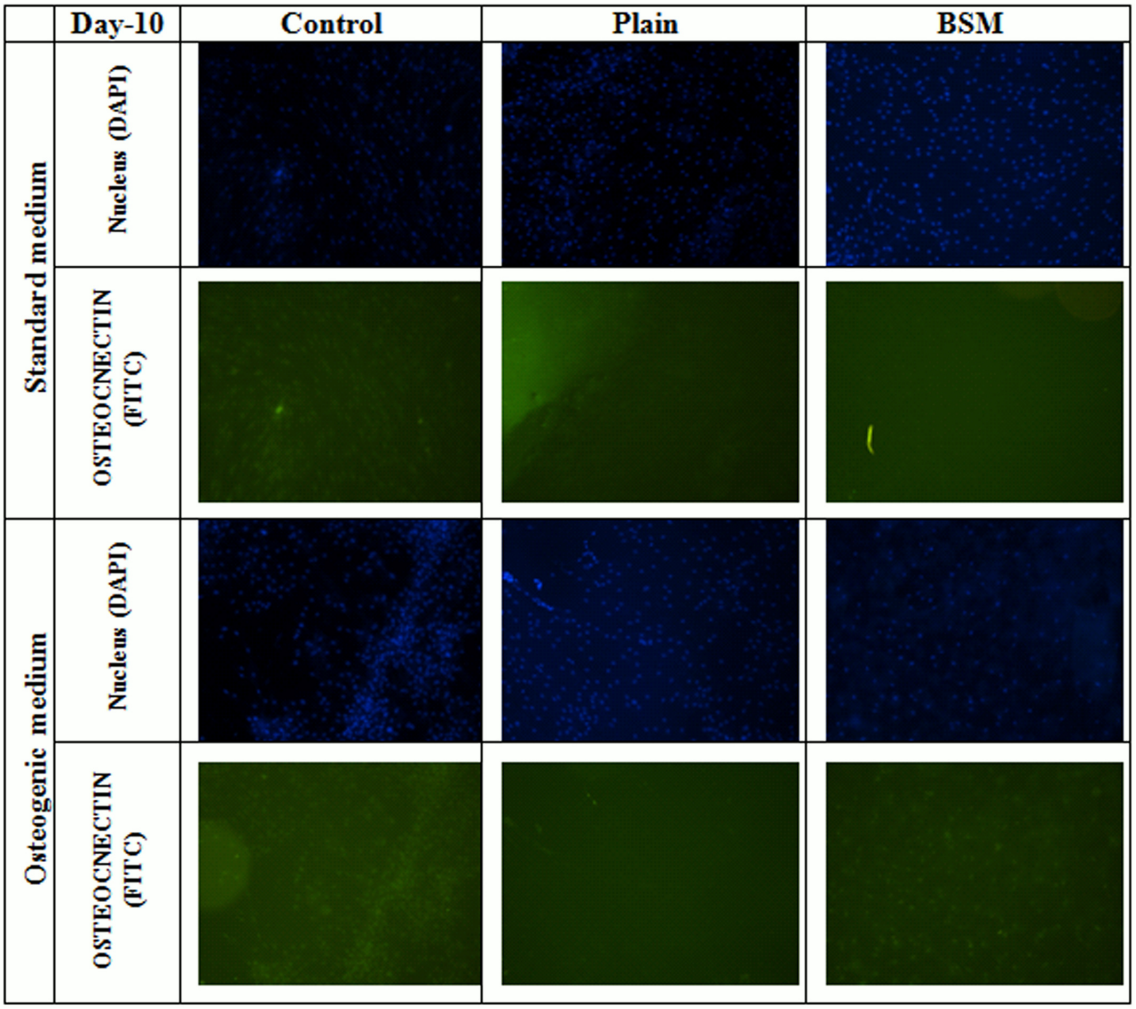

Figure 4.17 Differentiation capacity of human bone marrow mesenchymal stem cells on plain and BSM PLA labeled with anti-osteonectin antibody. Immunofluorescent images of hBM MSCs primed for 4 days and then differentiated for 10 days in the absence of a polymeric scaffolds (control, a-d); on the plain PLA (e-h); and on the bone surface mimicked PLA (i-l). magnification x 100.

5. DISCUSSION

Bone surface mimicked biodegradable PLA scaffolds have been synthesized by using solvent casting technique for the possible tissue engineering applications. Basically, fabrication parameters of scaffolds together with the bone and the PDMS mold have been optimized by SEM analysis. Surface topography of optimized PLA scaffolds has been analyzed with SEM, contact angle measurement and AFM. Chemical composition of PLA, model drug and drug loaded PLA were examined by FTIR. Degradation and drug release profile of PLA scaffolds were also studied. After this characterization process was completed, cell studies had been done with plain PLA and BSM PLA.

5.1 SEM Analysis

In SEM analysis, PDMS mimicking effectiveness, PLA concentration and casting time to mimic the bone surface were investigated. First of all, it should be noticed that PDMS has been used as a negative template of bone; so its SEM image was the mirror image of bone and SEM image of PLA was as same as the bone (Figure 4.1). According to this SEM analysis, the best mimicked scaffolds were obtained at 10% PLA concentration and 24 h casting time. In order to search for the effectiveness of mimicking procedure, same bone surface used for synthesizing PDMS mold for 5 times. SEM images have shown that there are no significant differences between 1st and 5th PDMS molds in terms of topography. Here, it has been clearly emphasized that PDMS and PLA were able to mimic bone surface microstructure. In literature, bone regeneration has been studied by designing 3D bone scaffolds [57, 58]. Rather than designing scaffolds having similar microenvironment with bone, Figure 4.1 also proves that it is possible to mimic bone surface microenvironment by using bone itself. Since the bone regeneration and modeling occur on the surface of bone [59], bone surface morphology is essential during healing process [60]. Therefore, mimicking the bone surface with PLA was a good approach and SEM analysis supported that bone and bone surface

mimicked PLA have the same surface topography.

In order to optimize PLA fabrication parameters, different concentration of PLA (2.5-10% (w/v) chloroform) and casting time (as evaporated-24 h) were applied to the preparation process of PLA at RT (Figure 4.2. and 4.3.). After characterization of bone surface mimicked PLA scaffolds by SEM, the best mimicked scaffolds were obtained at 10% PLA concentration and 24 hours casting time. 2.5% BSM PLA was too thin, so it was challenging to remove PLA from PDMS mold. 5% BSM PLA was good but it has some mimicking limitation when compared to 10% BSM PLA as it is seen in Figure 4.2. Although all the casting time parameters have a successful mimicking profile, 10% PLA on PMDS until the chloroform evaporated was not easy to remove from PDMS mold and after removing it, edge of the BSM PLA curled up. It means that chloroform seemed to evaporate but actually more time was needed to complete the process. Therefore, in order to be sure about mimicking procedure, 24h casting time was chosen according to our observations and literature [9].

In order to optimize PDMS effectiveness, same bone was used to synthesize PDMS molds for 5 times. The master bone and the PDMS molds were examined by SEM analysis (Figure 4.4). This SEM image shows 3 different regions of same bone and PDMS molds. As observed from the SEM images, same bone could have been used to mimic bone surface topography for 5 times. After obtaining PDMS effectiveness, same optimization process was done for BSM PLA by using same bone and same PDMS molds (as seen Figure 4.4). This time, 10% PLA was used to fabricate multiple BSM PLA using same bone and PDMS molds for 20 times (Figure 4.5 and 4.6) Morphologically, there are no significant differences between 1st and 20th positive PLA replica. By the knowledge of morphological significance between 1st and 20th positive PLA, BSM PLA production is easier in terms of quantity and time saving.

5.2 Wettability of PLA Scaffolds

Contact angle measurements were done with three different PLA scaffolds for each and taken from three different contact points. Contact angle values of 10% plain PLA and 2.5-10% BSM PLA were given in Table 4.1 and their contact angle images were given in Figure 4.7. Contact angle value of plain PLA was $65.88° \pm 8.32°$ which is similar with PLA surface of Zhu et al. study [61]. Contact angle values were increased as the concentration of PLA increased which means that the surface hydrophobicity was increased. The experimental results showed that contact angle were strongly affected by the surface roughness [62]. The standard deviation of bone surface mimicked PLA scaffolds was quite high due to the surface roughness. It could be also referred to increase of hydrophobicity of BSM PLA scaffolds surface [63]. Since the cell-material interaction is the first meet for attachment, adhesion and spreading and the quality of this first meet will affect the cell proliferation and differentiation capacity on contact with the scaffolds [64]. Therfore, the hydrophobic surfaces lead to cell attachment and protein adsorption positively, 10% BSM PLA scaffolds was again a better optimization for our study.

5.3 FTIR Analysis

The FTIR spectra of diclofenac, PLA and drug loaded PLA was given in Figure 4.8. Their corresponding FTIR peaks were also given in Table 4.2 and Table 4.3. In order to observe drug loaded PLA chemical composition, FTIR spectra was performed. When PLA was loaded with diclofenac, intensity of diclofenac aromatic secondary $N-H$ and diclofenac asymmetric $O=C-O^-$ peaks decreased while some of the PLA FTIR peaks did not change but shifted [54, 55]. Na^- salts peak which was at 1452 cm^{-1} was still seen at drug loaded PLA scaffolds FTIR spectra. Aromatic C-C peaks relating to diclofenac was overlapped with PLA FTIR spectra in this region so that resulted in broad region at drug loaded PLA FTIR spectra [65]. These results supports that diclofenac was loaded on PLA scaffolds.

5.4 Surface Roughness of Plain and BSM PLA Scaffolds

Plain and bone surface mimicked PLA roughness values were 1.70 nm and 6.48 nm, respectively. Bone surface mimicked PLA was rougher than plain PLA (Figure 4.9). According to the Palin et al. studies, bone surface has high roughness value which could be concluded as bone surface does not have homogenous roughness in nano-scale [50, 66]. Bone surface mimicked PLA may possess more advantageous than plain PLA in cell studies with regards to their surface roughness comparison [60].

5.5 In-vitro Degradation of PLA Scaffolds

The plain and bone surface mimicked PLA scaffolds lost their weight linearly during the initial weeks, before the rate of weight loss decreased as it is given in Figure 4.10. After degradation for 9 weeks, 7.38% $\pm$ 0.04% of the original weight from plain PLA and 5.19%$\pm$ 0.15% of bone surface mimicked PLA had been lost. PLA is degraded in vivo by hydrolysis and their degradation characteristics are affected some parameters such as molecular structure, crystallinity and L/D forms ratio, the greater the resorption time,hydrophilicity and sample size. Hence, PLA has long degradation time and it almost is up to 2 years [52]. According to weight loss results, hydrolytic degradation was really slow between weeks 3 and 7. After that bone surface mimicked PLA scaffolds degradation rate was increased. Although plain PLA scaffolds degradation rate was increased after 7 week, it seemed to slow down again. The reason of the difference between degradation curves could be the surface topography difference between these two scaffolds. According to Odelius et al., The solid and plain films and scaffolds revealed the fastest mass loss rate than the porous and rough scaffolds [67]. It can be concluded that surface area may affect the degradation rate of PLA scaffolds. Weight loss percentages are quite low because of the low degradation profile of PLA (up to 2 years) [68].

The SEM images of degradation in Figure 4.12 and Figure 4.11 were showed the morphologies of the plain and bone surface mimicked PLA in vitro degradation

after 2 and 4 weeks. Small morphological changes could be observed after one month degradation period [52].

5.6 Drug Release Studies

Cumulative drug release of drug loaded plain and drug loaded BSM PLA was shown in Figure 4.13. According to this release chart, both scaffolds had a same drug release profile although the amount of released drug was different. After 1 week, drug release for both scaffolds was slow down but significant differences could be observed from both scaffolds. It could be the reason for rapid release of drug from plain PLA could be that diffusion of the drug through the PBS solution was easy when it compared to the drug loaded BSM PLA scaffolds'. The slow degradation of the PLA allows slow release of the drug. Therefore, drug release seemed to be stopped after 2 weeks for both PLA scaffolds. In addition, drug release profile of plain and BSM PLA scaffolds were consistent with degradation of rate [21, 67, 69].

5.7 Cell Studies

One of the aim of this thesis is to investigate the effect of surface topography on hBM MSCs viabilility and differentiation using bone surface mimicked PLA scaffolds. The viability test showed that control grup, plain and bone surface mimicked PLA scaffolds demonstrated the same behavior. A little increase was observed in the number of the viable cells on bone surface mimicked PLA scaffolds. The results revealed PLA scaffolds were compatible with hBM MSCs and surface topography has little effect on the viability compared to control group and plain PLA. This result was expected for PLA scaffolds which is a well-known biocompatible polymer [46, 48, 56].

The osteogenic differentiation of BM hMSCs is guided with both systemic hormones (i.e. parathyroid hormone (PTH), estrogens, and glucocorticoids) and growth

factors (i.e. bone morphogenetic protein (BMP) family, transforming growth factor-beta (TGF-β), and fibroblast growth factor-2 (FGF-2)) [70]. With the guidance of these factors, specific intracellular signal pathways that modify the expression and activity of several transcription factors in hMSCs are activated, which result in osteoblastic differentiation rather than chondrocytic, adipocytic, or myogenic ones [70].

In order to investigate the differentiation capacity of human bone marrow mesenchymal stem cells on plain and bone surface mimicked PLA, they were treated with monoclonal anti-human collagen type I antibody and FITC conjugated secondary antibody for receptor staining at day-7 in standard and osteogenic medium. Since, Collagen I expression is a marker of early osteoblastic cells [70], from immunofluorescent images at day-7, we can conclude that, both in standard and osteogenic medium on plain and BSM PLA scaffolds, hBM MSCs possess a osteogenic differentiation profile. Obviously, higher osteogenic differentiation was observed in osteogenic medium. The surface topography and roughness affect the protein adsorption and the structure of the adsorbed proteins. That's why it can also be inferred that the collagen I expression of the bone marrow cells cultured on BSM PLA scaffolds in standart medium was influenced by microstructure and surface roughness of BSM PLA scaffolds [71]. hBM MSCs were treated with monoclonal anti-human osteocalcin and osteonectin antibody and FITC conjugated secondary antibody for receptor staining at day-10 in standard and osteogenic medium. There was no signs of osteocalsin and osteonectin expressions at day-10 from hBM MSCs since they are late markers of osteogenic differentition. The aim for us, looking for the relatively late markers of osteogenic differentiation markers such as osteocalsin and osteonection in future studies, to show if bone surface topography had an effect on osteogenic stem cell differentiation.

5.8 Future Studies

Basically, the findings of this thesis may be useful to understand the changing the characteristics of scaffolds such as surface hardness, chemical and biochemical content, surface roughness and topography affected cell-surface, cell-tissue scaffold interface characteristics, bone cell, stem cell and other cells' behavior and mechanisms.

Examining these cell behavior in a real-time using bioreactor might be one of the future aspects. For this reason, the synthesized PLA tissue scaffolds will be cultured adipose derived stem cells' and they will be directed to the bone cell differentiation and formation are going to be examined in vitro conditions and inside the bioreactor system.

APPENDIX A. CALIBRATION CURVE

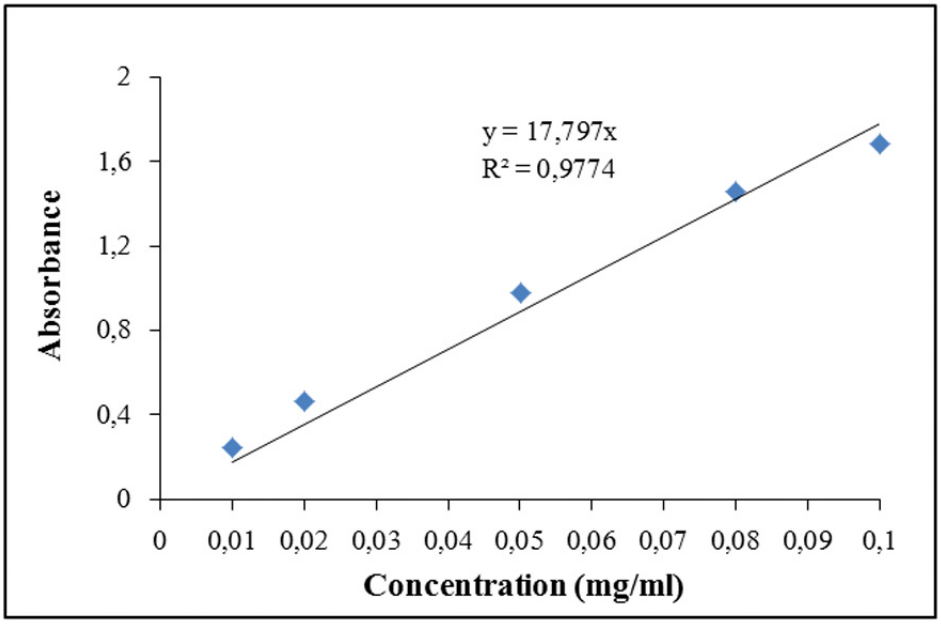

Figure A.1 Diclofenac calibration curve at 276 nm.

APPENDIX B. Flow Cytometric Analysis

Flow cytometric analyses of P3 BM-MSCs were performed on a FACS Aria flow cytometer (Becton, Dickinson Biosciences) to evaluate BM-MSCs in terms of expression of main MSC surface markers CD73 (BD Biosciences), CD90 (BD Biosciences), CD105(eBioscience) and lack of expression of hematopoietic stem cell markers CD34 (BD Biosciences). All markers were conjugated with either fluorescent isothiocyanate or phycoerythrin. BM-MSCs were trypsinized and washed with PBS. To evaluate BMMSCs marker profile, 1.5 x 105 suspended in 100 mL PBS-BSA- Na azide with 2 mL of each flow cytometry antibody in a separate tube and incubated for 30 min. in the dark. At the end of incubation, cells were washed twice with PBS and finally diluted in 200 mL PBS-BSA-Na azide. The analysis of cells was performed according to 10.000 event count with the FACS Aria. The acquired data was analyzed by using BD FACS Diva Software v6.1.2 (Beckon Dickinson Biosciences).

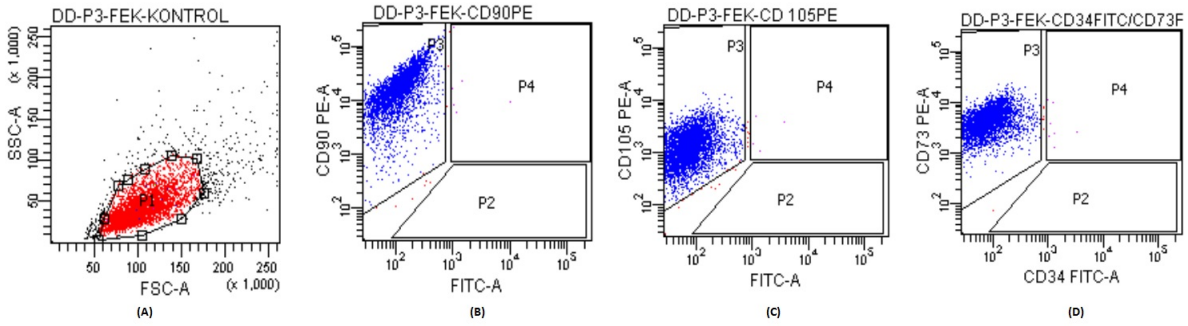

Figure B.1 Flow cytometric analyses of P3 BM-MSCs a) Control; b) CD90; c) CD105; d) CD73 markers expression.

B.1 Adipogenic and Osteogenic Differentiation

Adipogenic and osteogenic differentiation tests were performed to confirm that the cells used in the experiments were mesenchymal stem cells (MSCs). MSCs were grown to confluency (90-100%) on six-well plates, then, exposed to adipogenic medium consisting of LG-DMEM supplemented with 10% FBS, 1 μM dexamethasone, 60 μM indomethacin, 500 μM isobutylmethylxanthine, and 5 μg/mL insulin (Sigma Chemical Co.-Aldrich) for 21 days and stained with Oil Red O (Sigma Chemical Co.-Aldrich). MSCs were cultured for 21 days to 50-60% confluency and exposed to osteogenic induction medium consisting of LG-DMEM supplemented with 10% FBS, 100 nM dexamethasone, 10 mM β-glycerophosphate, and 0.2 mM ascorbic acid (Sigma Chemical Co.-Aldrich) for 21 days and stained with Alizarin Red S (Sigma Chemical Co.-Aldrich) (Control: Non-induced cells).

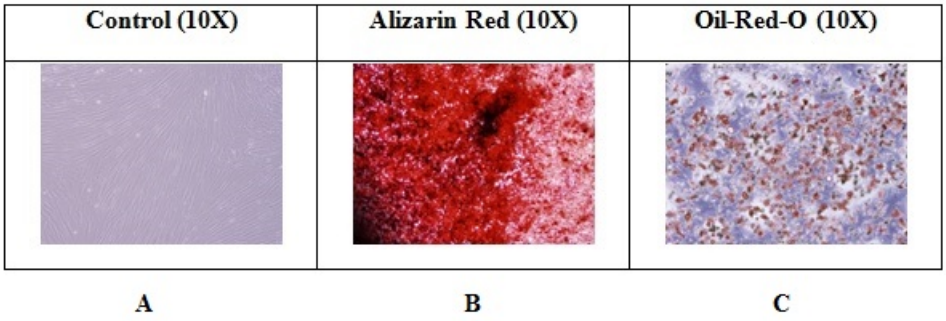

Figure B.2 Conformation of MSCs differentiation of A) Control, B) Alizarin Red, C) Oil-Red-O staining.

REFERENCES

1. Mortera-Blanco, T., N. Panoskaltsis, and A. Mantalaris, "Tissue engineering of normal and abnormal bone marrow," *Comprehensive Biotechnology*, Vol. 5, pp. 331–340, 2011.

2. Yua, F., X. C. L. Zenga, Q. Zhanga, and X. Chena, "An interpenetrating ha/g/cs biomimic hydrogel via diels-alder click chemistry for cartilage tissue engineering," *Carbohydrate Polymers*, Vol. 97, pp. 188–195, 2013.

3. Wang, Y., Y. Mo, M. Zhu, and M. Bai, "Wettability of metal coatings with biomimic micro textures," *Surface and Coatings Technology*, Vol. 203, pp. 137–141, 2008.

4. Yin, S., D. Wu, J. Yang, S. Lei, T. Kuang, and B. Zhu, "Fabrication and surface characterization of biomimic superhydrophobic copper surface by solution-immersion and self-assembly," *Applied Surface Science*, Vol. 257, pp. 8481–8485, 2011.

5. Davies, J., S. Haq, T. Hawke, and J. P. Sargent, "A practical approach to the development of a synthetic gecko tape," *International Journal of Adhesion and Adhesives*, Vol. 29, no. 4, pp. 380–390, 2009.

6. Liu, Y., and G. Li, "A new method for producing lotus effect on a biomimetic shark skin," *Journal of Colloid and Interface Science*, Vol. 388, pp. 235–242, Dec 2012.

7. Sharma, C. S., K. Abhishek, H. Katepalli, and A. Sharma, "Biomimicked superhydrophobic polymeric and carbon surfaces," *Ind. Eng. Chem. Res.*, Vol. 50, pp. 13012–13020, 2011.

8. Porter, J. R., T. T. Rucky, and K. C. Popat, "Bone tissue engineering: A review in bone biomimetics and drug delivery strategies," *Biotechnol. Prog.*, Vol. 25, pp. 1539–1560, Oct 2009.

9. Lu, Z., S.-I. R-Esfahani, G. Wang, and H. Zreiqat, "Bone biomimetic microenvironment induces osteogenic differentiation of adipose tissue-derived mesenchymal stem cells," *Nanomedicine: Nanotechnology, Biology, and Medicine*, Vol. 8, pp. 507–515, 2012.

10. Blom, A. W., V. Wylde, C. Livesey, M. R. Whitehouse, S. E-Waring, G. C. Bannister, and I. D. Learmonth, "Impaction bone grafting of the acetabulum at hip revision using a mix of bone chips and a biphasic porous ceramic bone graft substitute," *Acta Orthopaedica*, Vol. 80, no. 2, pp. 150–154, 2009.

11. Holzapfel, B. M., M. P. Chhaya, F. P. W. Melchels, N. P. Holzapfel, P. M. Prodinger, R. von E-Rothe, M. van Griensven, J.-T. Schantz, M. Rudert, and D. W. Hutmacher, "Can bone tissue engineering contribute to therapy concepts after resection of musculoskeletal sarcoma?," *Hindawi Publishing Corporation Sarcoma*, pp. 1–10, 2013.

12. Mitra, J., G. Tripathi, A. Sharmaa, and B. Basu, "Scaffolds for bone tissue engineering: role of surface patterning on osteoblast response," *RSV Adv.*, Vol. 3, pp. 11073–11094, 2013.

13. Sultana, N., *Biodegradable Polymer-Based Scaffolds for Bone Tissue Engineering*, Department of Biomechanics, Universiti Teknologi Malaysia, UTM, Skudai, 81310, Malaysia: Springer Berlin Heidelberg, 2013.

14. Burg, K. J. L., S. Porter, and J. F. Kellam, "Biomaterial developments for bone tissue engineering," *Biomaterials*, Vol. 21, pp. 2347–2359, 2000.

15. Chena, Q. Z., I. D. Thompsonb, and A. R. Boccaccini, "45s5 bioglass-derived glass-ceramic scaffolds for bone tissue engineering," *Biomaterials*, Vol. 27, pp. 2414–2425, April 2006.

16. Wen, C. E., Y. Yamada, K. Shimojima, Y. Chino, H. Hosokawa, and M. Mabuchii, "Novel titanium foam for bone tissue engineering," *J. Mater. Res.*, Vol. 17, no. 10, pp. 2633–2639, 2002.

17. Rodriguesa, C. V. M., P. Serricella, A. B. R. Linhares, R. M. Guerdesd, R. Borojevic, M. A. Rossie, M. E. L. Duarte, and M. Farina, "Characterization of a bovine collagen-hydroxyapatite composite scaffold for bone tissue engineering," *Biomaterials*, Vol. 24, pp. 4987–4997, Dec 2003.

18. Martino, A. D., M. Sittinger, and M. V. Risbud, "Chitosan: A versatile biopolymer for orthopaedic tissue-engineering," *Biomaterials*, Vol. 26, pp. 5983–5990, Oct 2005.

19. Rezwana, K., Q. Chena, J. Blakera, and A. R. Boccaccini, "Biodegradable and bioactive porous polymer/inorganic composite scaffolds for bone tissue engineering," *Biomaterials*, Vol. 27, pp. 3413–3431, 2006.

20. Dash, T. K., and V. B. Konkimalla, "Poly-e-caprolactone based formulations for drug delivery and tissue engineering: A review," *Journal of Controlled Release*, Vol. 158, pp. 15–33, 2012.

21. Roman, M. S. S., M. J. Holgado, B. Salinas, and V. Rives, "Drug release from layered double hydroxides and from their polylactic acid (pla) nanocomposites," *Clay Science*, Vol. 71, pp. 1–7, 2013.

22. Proikakis, C. S., P. A. Tarantili, and A. G. Andreopoulos, "The role of polymer/drug interactions on the sustained release from poly(dl-lactic acid) tablets," *European Polymer Journal*, Vol. 42, pp. 3269–3276, 2006.

23. Votteler, M., P. Kluger, H. Walles, and K. S-Layland, "Stem cell microenvironments - unveiling the secret of how stem cell fate is defined," *Micromolecular Bioscience*, Vol. 10, pp. 1302–1315, 2010.

24. Colencia, R., L. R. da S Assuncaob, S. R. M. Bomfimc, M. de A Golimd, E. Deffunee, and S. H. P. Oliveira, "Bone marrow mesenchymal stem cells stimulated by bfgf up-regulated protein expression in comparison with periodontal fibroblasts in vitro," *Archives of Oral Biology*, Vol. 59, pp. 268–276, March 2014.

25. Pittenger, M. F., A. M. Mackay, S. C. Beck, R. K. Jaiswal, R. Douglas, J. D. Mosca, M. A. Moorman, D. W. Simonetti, S. Craig, and D. R. Marshak, "Multilineage potential of adult human mesenchymal stem cells," *Science*, Vol. 284, pp. 143–147, April 1999.

26. El-Amina, S. F., H. H. Lua, Y. Khan, J. Burems, J. Mitchell, R. S. Tuanb, and C. T. Laurencina, "Extracellular matrix production by human osteoblasts cultured on biodegradable polymers applicable for tissue engineering," *Biomaterials*, Vol. 24, pp. 1213–1221, 2003.

27. Stevens, M. M., "Biomaterials for bone tissue engineering," *Materialstoday*, Vol. 11, pp. 17–25, May 2008.

28. Wehrli, F. W., "Structural and functional assessment of trabecular and cortical bone by micro magnetic resonance imaging," *Journal of Magnetic Resonance Imaging*, Vol. 25, pp. 390–409, 2007.

29. Downey, P. A., and M. I. Siegel, "Bone biology and the clinical implications for osteoporosis," *Physical Theraphy*, Vol. 86, p. 77, Jan 2006.

30. Pilitsis, J. G., D. R. Lucas, and S. R. Rengachary, "Bone healing and spinal fusion," *Neurosurg Focus*, Vol. 13, no. 6, pp. 1–11, 2002.

31. Hollinger, J. O., T. A. Einhorn, B. Doll, and C. Sfeir, eds., *Bone Tissue Engineering*, CRC, 2004.

32. Gu, C., D. R. Katti, and K. S. Katti, "Photoacoustic ftir spectroscopic study of undisturbed human cortical bone," *Spectrochimica Acta Part A: Molecular and Biomolecular Spectroscopy*, Vol. 103, pp. 25–37, 2013.

33. Rho, J.-Y., L. K-Spearing, and P. Zioupos, "Mechanical properties and the hierarchical structure of bone," *Medical Engineering and Physics*, Vol. 20, no. 2, pp. 92–102, 1998.

34. Hall, B. K., *Bones and Cartilage: Developmental Skeletal Biology*, Jordan Hill GBR: Academic Press, 2005.

35. Mckibbin, B., "The biology of fracture healing in long bones, from the department of traumatic and orthopaedic surgery," *The journal of bone and joint surgery*, Vol. 60-B, pp. 150–162, May 1978.

36. Healy, K. E., and R. E. Guldberg, "Bone tissue engineering," *J Musculoskelet Neuronal Interact*, Vol. 7, no. 4, pp. 328–330, 2007.

37. Liu, X., and P. X. Ma, "Polymeric scaffolds for bone tissue engineering," *Annals of Biomedical Engineering*, Vol. 32, pp. 477–486, March 2004.

38. Salgado, A. J., O. P. Coutinho, and R. L. Reis, "Bone tissue engineering: State of the art and future trends," *Macromol. Biosci.*, Vol. 4, pp. 743–765, 2004.

39. Jain, R. A., "The manufacturing techniques of various drug loaded biodegradable poly(lactide-co-glycolide) (plga) devices," *Biomaterials*, Vol. 21, pp. 2475–2490, Dec 2000.

40. Nejati, E., V. Firouzdor, M. B. Eslaminejad, and F. Bagheri, "Needle-like nano hydroxyapatite/poly(l-lactide acid) composite scaffold for bone tissue engineering application," *Materials Science and Engineering C*, Vol. 29, pp. 942–949, 2009.

41. Martino, S., F. DAngelo, I. Armentano, J. M. Kenny, and A. Orlacchio, "Stem cell-biomaterial interactions for regenerative medicine," *Biotechnology Advances*, Vol. 30, pp. 338–351, 2012.

42. Seong, J. M., B.-C. Kim, J.-H. Park, K. Kwon, A. Mantalaris, and Y.-S. Hwang, "Stem cells in bone tissue engineering," *Biomed. Mater.*, Vol. 5, pp. 1–15, 2010.

43. Marolt, D., M. Knezevic, and G. V. Novakovic, "Bone tissue engineering with human stem cells," *Stem Cell Research and Therapy*, Vol. 1, no. 10, pp. 1–10, 2010.

44. Özgürbüz, L. M., "Production of xenografts for hard tissue repair," Master's thesis, Hacettepe University, Ankara, Turkey, 2006.

45. Fredonnet, J., J. Foncy, S. Lamarre, J.-C. Cau, E. Trevisiol, J.-P. Peyrade, J. M. Francois, and C. Severac, "Dynamic pdms inking for dna patterning by soft lithography," *Microelectronic Engineering*, Vol. 111, pp. 379–383, 2013.

46. Umekia, N., T. Satob, M. Haradac, J. Takedad, S. Saitoe, Y. Iwaoa, and S. Itai, "Preparation and evaluation of biodegradable films containing the potent osteogenic compound bfb0261 for localized delivery," *International Journal of Pharmaceutics*, Vol. 404, pp. 10–18, Oct 2011.

47. Garipcan, B., S. Odabas, G. Demirel, J. Burger, S. S. Nonnenmann, M. T. Coster, E. M. Gallo, B. Nabet, J. E. Spanier, and E. Piskin, "In vitro biocompatibility of n-type and undoped silicon nanowires," *Advanced Biomaterials*, Vol. 13, no. 1-2, pp. 3–9, 2011.

48. Abdal-hay, A., F. A. Sheikhc, and J. K. Limb, "Air jet spinning of hydroxyapatite/poly(lactic acid) hybrid nanocomposite membrane mats for bone tissue engineering," *Colloids and Surfaces B: Biointerfaces*, Vol. 102, pp. 635–643, 2013.

49. Wu, F., J. Wei, C. Liu, B. O'Neill, and Y., "Fabrication and properties of porous scaffold of zein/pcl biocomposite for bone tissue engineering," *Composites*, Vol. 43, pp. 2192–2197, 2012.

50. Palin, E., H. Liu, and T. J. Webster, "Mimicking the nanofeatures of bone increases bone-forming cell adhesion and proliferation," *Nanotechnology*, Vol. 16, pp. 1828–1835, 2005.

51. Shi, Q., C. Zhou, Y. Yue, W. Guo, Y. Wu, and Q. Wu, "Mechanical properties and in vitro degradation of electrospun bio-nanocomposite mats from pla and cellulose nanocrystals," *Carbohydrate Polymers*, Vol. 90, pp. 301–308, May 2012.

52. Gong, Y., Q. Zhou, C. Gao, and J. Shen, "In vitro and in vivo degradability and cytocompatibility of poly(l-lactic acid) scaffold fabricated by a gelatin particle leaching method," *Acta Biomaterialia*, Vol. 3, pp. 531–540, 2007.

53. Çelebi, B., A. E. Elçin, and Y. M. Elçin, "Proteome analysis of rat bone marrow mesenchymal stem cell differentiation," *J Proteome Res*, Vol. 9, pp. 5217–5227, Oct 2010.

54. Shivakumar, H. N., B. G. Desai, and G. Deshmukh, "Design and optimization of diclofenac sodium controlled release solid dispersions by response surface methodology," *Indian J Pharm Sci.*, Vol. 70, pp. 22–30, Jan-Feb 2008.

55. Copinet, A., C. Bertrand, S. Govindin, V. Coma, and Y. Couturier, "Effects of ultraviolet light (315 nm), temperature and relative humidity on the degradation of polylactic acid plastic films," *Chemosphere.*, Vol. 55, pp. 763–773, Nov 2004.

56. Kroeze, R. J., M. N. Helder, L. E. Govaert, and T. H. Smit, "Biodegradable polymers in bone tissue engineering," *Materials*, Vol. 2, pp. 833–856, 2009.

57. Adachi, T., Y. Osako, M. Tanaka, M. Hojo, and S. J. Hollister, "Framework for optimal design of porous scaffold microstructure by computational simulation of bone regeneration," *Biomaterials*, Vol. 27, pp. 3964–3972, 2006.

58. Lin, C. Y., N. Kikuchi, and S. J. Hollister, "A novel method for biomaterial scaffold internal architecture design to match bone elastic properties with desired porosity," *Jornal of Biomechanics*, Vol. 37, pp. 623–636, 2004.

59. Deng, H. W., Y. Z. Liu, and C. Y. Guo, eds., *Current Topics in Bone Biology*, River Edge NJ USA: World Scientific Publishing Co., 2005.

60. Wennerberg, A., and T. Albreaktsson, "Effects of titanium surface topography on bone integration: a systematic review," *Clin. Oral Impl. Res.*, Vol. 20, pp. 172–184, 2009.

61. Zhu, A., M. Zhang, J. Wu, and J. Shen, "Covalent immobilization of chitosan/heparin complex with a photosensitive hetero-bifunctional crosslinking reagent on pla surface," *Biomaterials*, Vol. 23, pp. 4657–4665, 2002.

62. Miwa, M., A. Nakajima, A. Fujishima, K. Hashimoto, and T. Watanabe, "Effects of the surface roughness on sliding angles of water droplets on superhydrophobic surfaces," *Langmuir*, Vol. 16, pp. 5754–5760, 2000.

63. Bonzani, I. C., R. Adhikari, S. Houshyar, R. Mayadunne, P. Gunatillake, and M. M. Stevens, "Synthesis of two-component injectable polyurethanes for bone tissue engineering," *Biomaterials*, Vol. 28, pp. 423–433, Sep 2007.

64. Anselme, K., "Osteoblast adhesion on biomaterials," *Biomaterials*, Vol. 21, pp. 667–681, April 2000.

65. Bartolomei, M., P. Bertocchi, E. Antoniella, and A. Rodomonte, "Physico-chemical characterisation and intrinsic dissolution studies of a new hydrate form of diclofenac sodium: comparison with anhydrous form," *Journal of Pharmaceutical and Biomedical Analysis*, Vol. 40, pp. 1105–1113, 2006.

66. Hassenkam, T., G. E. Fantner, J. A. Cutroni, J. C. Weaver, D. E. Morse, and P. K. Hansma, "High-resolution afm imaging of intact and fractured trabecular bone," *Bone*, Vol. 35, pp. 4–10, 2004.

67. Odelius, K., A. Hoglund, S. Kumar, M. Hakkarainen, A. K. Ghosh, N. Bhatnagar, and A. C. Albertsson, "Porosity and pore size regulate the degradation product profile of polylactide," *Bio Macromoleculus*, Vol. 12, pp. 1250–1258, 2011.

68. Grizzi, I., H. Garreau, S. Li, and M. Vert, "Hydrolytic degradation of devices based on poly[m-lactic acid) sizedependence," *Biomaterials*, Vol. 16, pp. 305–311, 1995.

69. Agnihotri, S. M., and P. R. Vavia, "Diclofenac-loaded biopolymeric nanosuspensions for ophthalmic application," *Nanomedicine: Nanotechnology, Biology, and Medicine*, Vol. 5, pp. 90–95, 2009.

70. Giuliani, N., G. Lisignoli, M. Magnani, C. Racano, M. Bolzoni, B. D. Palma, A. Spolzino, C. Manferdin, C. Abati, D. Toscani, A. Facchini, and F. Aversa, "New insights into osteogenic and chondrogenic differentiation of human bone marrow mesenchymal stem cells and their potential clinical applications for bone regeneration in pediatric orthopaedics," *Hindawi Publishing Corporation Stem Cells International*, pp. 1–11, 2013.

71. Deligianni, D. D., N. D. Katsala, P. G. Koutsoukos, and Y. F. Missirlis, "Effect of surface roughness of hydroxyapatite on human bone marrow cell adhesion, proliferation, differentiation and detachment strength," *Biomaterials*, Vol. 22, no. 1, pp. 87–96, 2000.